ELSEVIER

Journal of Marine Systems 36 (2002) 239–267

JOURNAL OF MARINE SYSTEMS

www.elsevier.com/locate/jmarsys

Planktonic community structure and carbon cycling in the Arabian Sea as a result of monsoonal forcing: the application of a generic model

J.C. Blackford *, P.H. Burkill[1]

Plymouth Marine Laboratory, Prospect Place, PL1 3DH, Plymouth, UK

Received 9 March 2001; accepted 20 June 2002

Abstract

The Arabian Sea exhibits a complex pattern of biogeochemical and ecological dynamics, which vary both seasonally and spatially. These dynamics have been studied using a one-dimensional vertical hydrodynamic model coupled to a complex ecosystem model, simulating the annual cycle at three contrasting stations. These stations are characterised by seasonally upwelling, mixed-layer-deepening and a-seasonal oligotrophic conditions, respectively, and coincide with extensively measured stations on the two JGOFS ARABESQUE cruises in 1994. The model reproduces many spatial and temporal trends in production, biomass, physical and chemical properties, both qualitatively and quantitatively and so gives insight into the main mechanisms responsible for the biogeochemical and ecological complexity. Monsoonal systems are typified by classical food web dynamics, whilst intermonsoonal and oligotrophic systems are dominated by the microbial loop. The ecosystem model (ERSEM), developed for temperate regions, is found to be applicable to the Arabian Sea system with little reparameterisation. Differences in in-situ physical forcing are sufficient to recreate contrasting eutrophic and oligotrophic systems, although the lack of lateral terms are probably the greatest source of error in the model. Physics, nutrients, light and grazing are all shown to play a role in controlling production and community structure. Small-celled phytoplanktons are predicted to be dominant and sub-surface chlorophyll maxima are robust centers of production during intermonsoon periods. Analysis of carbon fluxes indicate that physically driven outgassing of CO_2 predominates in monsoonal upwelling systems but ecological activity may significantly moderate CO_2 outgassing in the Arabian Sea interior.

Keywords: Ecological modeling; Arabian Sea; Carbon cycle; Plankton community; 1D water column model

1. Introduction

The Arabian Sea (Fig. 1) is an unusual and complex ocean basin. Bounded to the north, west and east by land and exceeding depths of 4000 m and although tropical, the basin is continually influenced by the seasonally reversing monsoonal winds (Swallow,

* Corresponding author. Tel.: +44-1752-633468; fax: +44-1752-633101.

E-mail address: jcb@pml.ac.uk (J.C. Blackford).

[1] Present address: Southampton Oceanography Centre, University of Southampton, Waterfront Campus, Southampton SO14 3ZH, UK.

0924-7963/02/$ - see front matter © 2002 Elsevier Science B.V. All rights reserved.
PII: S0924-7963(02)00182-3

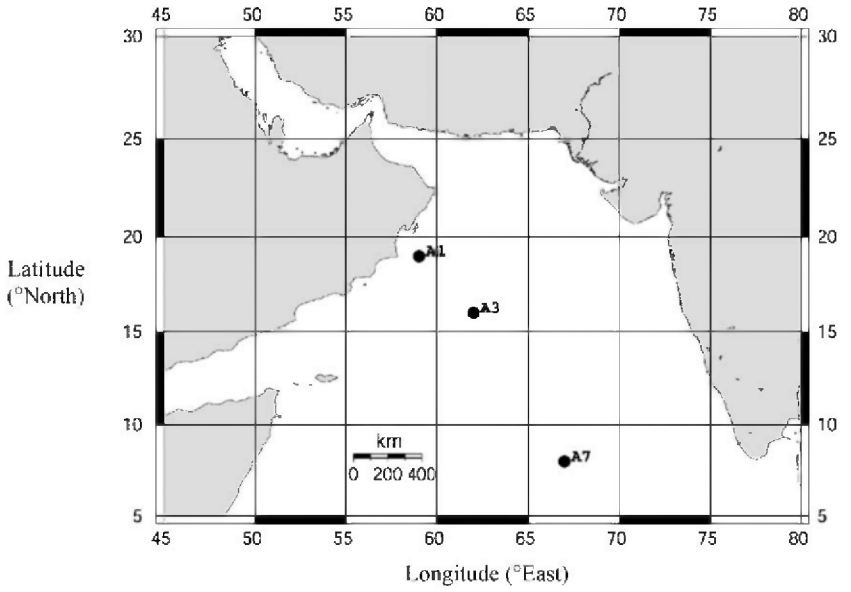

Fig. 1. Geographical position of the modelled stations in the Arabian Sea.

1991). These winds produce complete reversal of the surface currents and generate a range of contrasting oceanographic conditions (Burkill et al., 1993a). Thus surface conditions can range from eutrophy driven by seasonal upwelling through to oligotrophy generated by aseasonal strong stratification (Yoder et al., 1993). Between June and September, the South West Monsoon (SWM) blows as the concentrated, low-level Findlater Jet (Findlater, 1974). This creates strong Ekman transport that induces upwelling of inorganically rich deep water in the north–west of the region (Kindle, 2002), with downwelling and mixed layer deepening observed to the south–east of the jet. Although more moderate, the North–East Monsoon (NEM, December–February) also entrains deep water into the photic zone. By contrast, the inter-monsoon periods, with weak and variable winds permit the development of well-stratified systems largely devoid of nutrients in the surface layer. In the south of the region, away from the influence of the monsoon winds, seasonal mixing is slight, with thermal stratification and a deep nutricline predominating throughout the year (Schott and McCreary, 2001).

SWM induced upwelling has been considered to generate the highest rates of primary production while the NEM has been thought to be biologically less dynamic. Much of this understanding has arisen from satellite derived, ocean colour images of the basin. These have shown accumulation of high chlorophyll concentrations at the end of the SWM with lower concentrations at other times (Banse and English, 2000). For the main SWM period, satellite information has been poor because of the dense monsoon cloud base and the difficulties of working at sea during the monsoon. To better understand the system particularly at this time, international biogeochemical process studies were planned as part of the Joint Global Ocean Flux Study, and the results are now being published, for example in Deep-Sea Research (Burkill et al., 1993a,b; Van Weering et al., 1997; Smith, 1998, 1999, 2000, 2001; Burkill, 1999a; Gage et al., 2000; Pfannkuche and Lochte, 2000) with a synthesis report produced by Watts et al. (2002). Some of the results from these studies are surprising. Although we now know that primary production can reach 4 g C m^{-2} day^{-1} in the vicinity of the Omani coast at the end of SWM (Savidge and Gilpin, 1999), production during the SWM can be lower than during the main NEM period in the North East of the region (Marra et al., 1998; Gunderson et al., 1998) where deep convective mixing due to cold winds blowing off the Indian subcontinent can generate production rates that average more than 1 g C m^{-2} day^{-1} over the season (Wiggert et al., 2000). Similarly experimental studies at sea have shown that

phytoplankton growth rates were similar during both monsoons (Landry et al., 1998).

During the stratified inter-monsoonal periods deep chlorophyll maxima are observed at depths of 40–60 m. In the offshore, oligotrophic regions, deep chlorophyll maxima are observed typically at around 80 m (Savidge and Gilpin, 1999). In oligotrophic areas and during the intermonsoon, the ecological community is dominated by smaller cells (Jochem et al., 1993; Burkill et al., 1993b) and recycling of carbon and nutrients within the photic zone is also observed to be an important feature. During the monsoons, large cells such as diatoms and subsequently their meso-grazers contribute more to cycling (Owens et al., 1993; Tarran et al., 1999). Also of importance is the exudation of dissolved organic carbon (DOC) and subsequent secondary production via bacterial utilisation, which, although less variable, plays a significant part in carbon cycling in the region (Pomroy and Joint, 1999; Ducklow, 1993).

The biogeochemical response to the seasonally reversing monsoonal forcing is complex. Studies on carbon dioxide in the Arabian Sea have shown a substantial increase in dissolved inorganic carbon in the coastal regions due to strong upwelling in the SW monsoon. This was also accompanied by very high CO_2 partial pressures in surface waters (Mintrop et al., 1999), which enhance the flux of carbon dioxide to the atmosphere. High wind speeds also increase the rate of exchange between atmosphere and ocean. The high rates of primary production, and its subsequent respiration or decomposition, may however influence CO_2 levels in the photic zone. Physically mediated changes in salinity and the biological influence on total alkalinity via N speciation may also act to modify pCO_2 in surface waters. In well-mixed regions that experience downwelling, the high levels of entrainment driven primary production may lead to CO_2 drawdown. Where Ekman pumping is slight or absent and surface primary production small, air–sea fluxes may be less significant. Sinking of a significant proportion of production is also observed (Buesseler et al., 1998), seemingly associated with large cell communities in the wake of monsoon events. Garrison et al. (2000) states that considerable evidence links carbon cycling and export to food web structure.

This study aims, by use of a coupled ecosystem-physical model, to reproduce the ecological observations and quantify the biogeochemical fluxes of carbon in the Arabian Sea as they vary on both seasonal and spatial scales. Given the complexity exhibited by this system it is important to use an ecosystem model

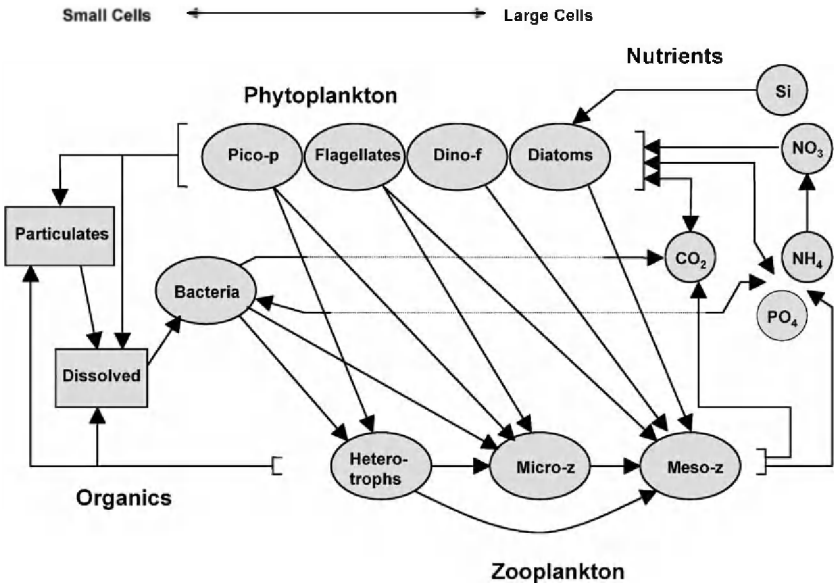

Fig. 2. The ecosystem model flow diagram indicating the carbon and nutrient pathways between the functional groups.

capable of reproducing the variety of food web structures found in the region. Hence the choice of the European Regional Seas Ecosystem Model (ERSEM, Baretta et al., 1995; Fig. 2) that simulates the cycling of carbon, nitrogen, phosphorous and silicon within size-resolved phytoplankton and zooplankton communities and the microbial loop. In this respect, the study extends on previous modelling of the region that has employed simpler representations of the ecosystem (e.g. McCreary et al., 1996; Keen et al., 1997; Ryabchenko et al., 1998; McCreary et al., 2001). The compromise employed here, in order to keep the study computationally tractable, but also due to the lack of boundary conditions is to confine the study to a finally resolved 1D vertical physical model and omit all horizontal processes with the exception of upwelling. Although this lack of horizontal terms is a significant omission form the model, studies have shown that local forcing is the dominant mediator of water column dynamics in the region during all but the latter stages of the southwest monsoon (Fischer, 2000; Rochford et al., 2000).

A number of questions are also posed by this study. Firstly, can the ecological model, developed for temperate systems, reproduce the dynamics of the Arabian Sea system? Secondly, to what extent can differences in in-situ physical forcing generate the complex trends in community structure across the region without recourse to advective mechanisms? Thirdly, what mechanisms cause specific community types to establish? Finally, does regional productivity influence the Arabian Sea's ability to be a source or sink of CO_2?

The coupled model has been applied to three contrasting stations in the Arabian Sea (Fig. 1, Table 1), which range from seasonally upwelling to near a-seasonal oligotrophy. These stations were extensively sampled by the two UK JGOFS "Arabesque" cruises held in 1994 as part of the international JGOFS Arabian Sea Process Study (Burkill, 1999b). The first cruise sampled the late SWM period, whilst the second cruise sampled the autumn inter-monsoon and early Northeast monsoon transition (INEM cruise). Whilst the goal is to replicate and elucidate the Arabesque cruises data set, reference is also made to the 1994–1996 US JGOFS Arabian Sea expedition (Smith et al., 1998a), which sampled a qualitatively similar transect from the coast of Oman to the Oceanic interior. Results from the US JGOFS and ARABESQUE cruises are generally qualitatively and quantitatively similar (Garrison et al., 2000).

Table 1
Space–time coordinates of the modelled Arabesque cruise stations

Station	Latitude (°N)	Longitude (°E)	Depth	Arabesque cruise: dates on station, 1994	
				C210	C212
A1	19	59	3397	4–7 Sept., 30 Sept.	21–26 Nov.
A3	16	62	3927	13–14 Sept., 28 Sept.	30–6 Nov/Dec.
A7	8	67	4705	19–21 Sept.	10–13 Dec.

The physical model system utilises the equations of the Mellor–Yamada turbulence closure model and the vertical diffusion submodel of the Princeton Ocean Model (Blumberg and Mellor, 1980; Mellor and Yamada, 1982). This coupled Princeton/Mellor–Yamada/ERSEM model has been applied successfully to water columns in the Adriatic (Allen et al., 1998; Vichi et al., 1998a,b) and the Mediterranean Sea (Allen et al., in press), but not previously to tropical regions.

2. The model

2.1. Physics and physical forcing

The Princeton/Mellor–Yamada physical model determines vertical temperature, turbulent kinetic energy and diffusion coefficient profiles. The model is forced by sea surface temperature, salinity and wind stress fields for 1994. Surface wind vectors are taken from the ECMWF (European Centre for Medium-range Weather Forecasts) model with a resolution of 12 h (Fig. 3). Daily values of sea surface temperature are derived from the Comprehensive Ocean Atmosphere Data Set (COADS) using monthly mean values averaged over the years 1993–1995. The inaccuracy in modelled surface heat flux data (Weller et al., 1998) and lack of a measured time series has precluded its use here. Surface salinities are derived from the US JGOFS database using qualitatively similar stations (Table 2). Incident solar radiation is calculated as a function of latitude and day length (Dobson and Smith, 1988), modified by monthly mean values of cloud cover again derived from the COADS 1993–1995 data set. Background light extinction coefficients have been

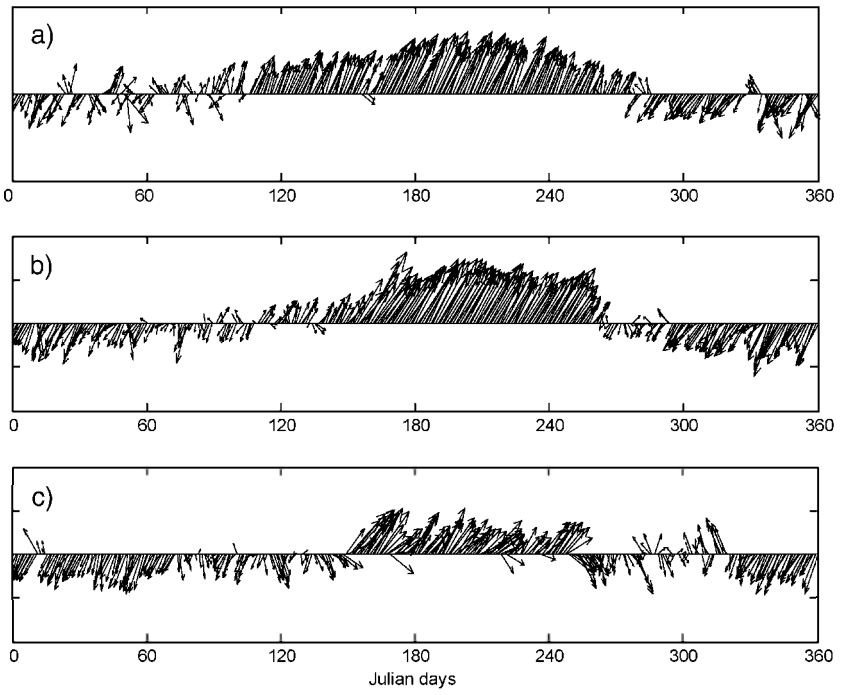

Fig. 3. Annual cycle of wind speed and direction for (a) station A1, (b) A3, (c) A7, as derived from the ECMWF model. Due North equates to vertically upwards, West to the left, etc.

chosen to fit the 1% light depths measured on station (Table 2).

The physical model considers the top 200 m of the water column divided into 40 equal layers of 5 m. The lower boundary is considered to be adiabatic with the exception of nutrients, CO_2, O_2, temperature and salinity, which are held to constant values (Table 2). At the upper boundary atmospheric exchange of CO_2 and O_2 are modelled. The partial pressure of CO_2 in the atmosphere is parameterised from Goyet et al. (1998) in the range 335.0–355.0 μatm with minimum values recorded from October to December and maximum values recorded in January and February. Carbonate chemistry and the partial pressure of CO_2 in the water are calculated using the equations described in Taylor et al. (1991), which utilise the Hansson (1973) equilibrium coefficients and Weiss' (1974) calculation of CO_2 solubility. In the absence of modelled pH, salinity normalized total alkalinity is taken from Millero et al. (1998) (NTA = 2290 μmol kg^{-1}) and modified according to the surface salinity. Gas transfer piston velocity is parameterised from Liss and Merlivat (1986), which differentiates between a smooth surface regime (wind speed < 3.6 m s^{-1}), a rough surface regime (3.6–13.0 m s^{-1}) and breaking waves (>13.0 m s^{-1}). Oxygen saturation is calculated from the formula of Weiss (1970) whilst the surface aeration rate uses the empirical formula described in Allen et al. (1998).

In order to reproduce the Ekman derived upwelling observed in the region for station A1, an additional vertical velocity has been parameterised from wind speed and direction. The Princeton model derives horizontal velocities for each layer (I) which may be equated to a lateral loss of water mass (A_I), a proportion of which (p) is replaced by water upwelling from below, the remainder by lateral advective gains. So for each layer, with U_I representing upwelling loss and U_{I-1} upwelling gain:

$$U_{I-1} = U_I + pA_I$$

The constant p is chosen to give appropriate vertical upwelling velocities, in this case 2 m day^{-1} at 100 m from Shi et al. (2000). Upwelling is assumed to occur

Table 2
Physical parameters and boundary conditions applied to each modelled station

	Unit	Station		
		A1	A3	A7
Physical				
Background viscosity	μmol	1.0e − 5	1.0e − 5	1.0e − 5
Background extinction	m^{-1}	0.04	0.04	0.04
Background silt	$mg \cdot m^{-3}$	750.0	350.0	250.0
Surface				
pCO_2 (air)	μ atm	350.0	350.0	350.0
Salinity max	psu	36.40	36.50	36.65
Salinity min	psu	35.70	36.00	35.25
Lower boundary				
Temperature	°C	15.0	15.0	14.0
Salinity	psu	35.8	35.8	35.3
Oxygen	$mmol \cdot m^{-2}$	5.0	5.0	10.0
Carbon dioxide	$mmol \cdot m^{-2}$	2250.0	2250.0	2250.0
Phosphate	$mmol \cdot m^{-2}$	2.30	2.30	2.30
Nitrate	$mmol \cdot m^{-2}$	25.0	25.0	25.0
Ammonium	$mmol \cdot m^{-2}$	0.0	0.0	0.0
Silicate	$mmol \cdot m^{-2}$	30.0	30.0	30.0

only when wind direction veers within 18° of true south–west. This reproduces the observed seasonal signal of upwelling in the region well (Halpern et al., 1998; Rixen et al., 2000). The resulting upwelling velocities for station A1 develop from May, peak in July and subside by mid-September. The resulting change in concentration for any state variable (C_I) is therefore given by:

$$\Delta C_I = U_{I-1} \times C_{I-1} - (U_I + pA_I) \times C_I$$

Thus simulations including upwelling are not conservative and experience horizontal loss terms as well as vertical gains. The simulation of downwelling is more problematic as horizontal boundary conditions are vital to formulating inputs to the system. With this information unavailable a simulation of downwelling has not been attempted.

2.2. Wind forcing

The ECMWF model provides a realistic spatial and temporal distribution of wind vectors for the Arabian Sea basin (Weller et al., 1998) (Fig. 3), which are in close agreement with the winds measured during the Arabesque cruises (Burkill, 1999b). These wind patterns are the primary influence on the physical structure of the water column, its seasonality and hence ecological activity.

At station A1 (Fig. 3a), the (ECMWF model) SW monsoon initially forms in May and following a breakdown in early June becomes established from mid-June onwards. Wind speeds exceed 13 $m\ s^{-1}$ for the remainder of June, July and the first half of August, thereafter dropping steadily, although the jet maintains its direction until mid-September. The inter-monsoon lasts only a month with the NE wind pattern establishing itself by mid-October, breaking down in early December and thereafter intermittent until the end of January. Wind speeds are significantly less when compared with the SW monsoon. At station A3 (Fig. 3b), the SW monsoon starts earlier, lasts longer and has consistently higher wind speeds (>15 $m\ s^{-1}$) than at A1. Additionally the NE monsoon has faster mean wind speeds and is more consistent than at A1. At station A7 (Fig. 3c), wind speeds are low and the SW monsoon much less distinct than at either stations A1 or A3.

2.3. The ecosystem model

The ecosystem model applied here is the ERSEM model (Baretta et al. 1995, Fig. 2) which has been applied in a variety of physical contexts from 1D to 3D including the North Sea (Patsch and Radach, 1997; Lenhart et al., 1997; Broekhuizen et al., 1995), the Adriatic Sea (Allen et al., 1998; Vichi et al., 1998a,b) and the Mediterranean Sea (Zavaterelli et al., 2000; Allen et al., in press). For this study, the pelagic components of ERSEM have been used. These and the modifications specific to the Arabian Sea study are briefly described. A mathematical description of ERSEM can be found in the two ERSEM special issues (Baretta et al., 1995; Ebenhöh et al., 1997 and subsequent papers), the World Wide Web (http://www.pml.ac.uk/ecomodels/ersem.htm) and particularly in the individual papers cited below.

ERSEM is conceived as a generic model, which when applied on a basin scale should be capable of correctly simulating the spatial pattern of ecological fluxes throughout the seasonal cycle and across eutrophic to oligotrophic gradients (Baretta-Bekker et al., 1997). The model uses three principle units

of currency—carbon, nitrogen and phosphorus—with each functional group containing these three pools. The inclusion of the silicate cycle allows a distinction between diatom and non-diatom production. Inorganic nitrogen is sub-divided into ammonium and nitrate compartments enabling the distinction between new and recycled production.

Four functional groups describe the phytoplankton, nominally picophytoplankton characterised as less than 2 μm diameter, flagellates (between 2 and 20 μm), dinoflagellates (greater than 20 μm) and diatoms. Phytoplankton dynamics are mediated by photosynthesis (as a function of temperature and light availability), respiration (both basal and active), excretion (nutrient-stressed and active), lysis, mortality and predation. Phytoplankton contain internal nutrient pools and thus varying C/N/P ratios. Nutrient uptake is a function of the difference between the internal and external pools (Ebenhöh et al., 1997).

Two size classes, the micro- and mesozooplankton represent zooplankton. The processes of ingestion, respiration, excretion and mortality contribute to the overall growth rate of the population. Microzooplankton, with variable internal C/N/P ratios (Baretta-Bekker et al., 1995, 1997) predate on picophytoplankton, flagellates and bacteria, whilst the mesozooplankton compete for flagellates but also predate on the diatoms and dinoflagellates. Mesozooplankton are treated as a biomass based predation model, identical in construct to the microzooplankton description. Given the lack of diurnal processes and the lack of dynamic mesozooplankton predators in the current application the case for developing a vertical migration mesozooplankton model is slight. Further, given the consistent warm temperatures in the region, it is hypothesised that mesozooplankton are more responsive than populations in cold temperate regions (Roman et al., 2000) and so are more readily modelled by a simple biomass approach.

Excretion and lysis products from all the ecological functional groups appear as both dissolved and particulate organic matter (DOM and POM), each of which are here sub-divided into two classes. The particulates are divided into large and small categories, the larger plankton (mesozooplankton, diatoms, dinoflagellates, microzooplankton) contribute to the large POM class with the smaller plankton producing the smaller POM. The smaller POM is considered to be more readably degradable by bacteria, due to a higher surface area to volume ratio) and has a lower sedimentation rate than its larger counterpart. The dissolved fraction is divided into labile and semi-labile fractions, with DOM production being divided equally into each. This allows at least a crude representation of the range of organic compounds in the dissolved fraction, some of which may be directly taken up by bacteria, some of which requires further degradation before bacterial utilization. Parameters relating to POM and DOM are included in Table 3.

Bacteria and heterotrophic flagellates represent the microbial loop (Baretta-Bekker et al., 1995, 1997). Bacteria utilise labile DOM and are also responsible for the degradation of POM to DOM. Semi labile DOM is considered to become labile at the rate of 1% per day. Bacteria compete with phytoplankton for nutrients and are predated by heterotrophic flagellates

Table 3
Bacteria model parameters

Description	Unit	Bacteria
Assimilation rate at 10 °C	day^{-1}	8.38
Half saturation oxygen limitation	–	0.3125
Fraction of small detritus available for B1	–	0.05
Fraction of large detritus available for B1	–	0.005
Assimilation efficiency	–	0.4
Assimilation efficiency at low oxygen concs	–	0.2
Basal respiration at 10 °C	day^{-1}	0.3
Mortality rate	day^{-1}	0.05
Max cell-quotum N	mmol N $(mg\ C)^{-1}$	0.0126
Max cell-quotum P	mmol P $(mg\ C)^{-1}$	0.000786
Michaelis constant for P uptake	mmol P m^{-3}	0.5
Michaelis constant for N uptake	mmol N m^{-3}	1.0
C/N ratio (Redfield)	–	6.625
Dissolution of dissolved organics to inorganics	day^{-1}	0.05
Relative nitrification rate	day^{-1}	0.05
Sediment conc for 0.01 day^{-1} nitrification rate	mg m^{-3}	2000.0
Rate of conversion of semi-labile to labile DOM	day^{-1}	0.01
Sedimentation rate of large POM class	m day^{-1}	7.5
Sedimentation rate of small POM class	m day^{-1}	0.3

Table 4
Optical phytoplankton parameters

Description	Unit	Value
Minimum value of optimal irradiance	w m^{-2}	4.00
Maximum daily shift in optimal irradiance	–	0.25
Photosynthetically available irradiance	–	0.50
Adaptation depth	m	10.00

that are in turn grazed by the larger zooplankton. All the consumers are also considered to graze within their functional group and pseudo cannibalistic terms are included. Fig. 2 summarises the interactions of the functional groups. Ecosystem parameters are given in Tables 3–7.

The simulations have been made using SESAME (Software Environment for Simulation and Analysis of Marine Ecosystems; Ruardij et al., 1995). The physical model uses a semi-implicit finite difference scheme forward in time and centered in space. The net transport of the biological variables are calculated using the physical model and then passed into SESAME where they are integrated along with the biogeochemical rates of change using a variable time step Euler method.

2.4. Initial conditions

Starting with vertical distributions of physics, chemistry and biology derived from literature and cruise data, each modelled water column has been run for at least 20 years using repeating forcing functions in order to remove any perturbations due to initial conditions.

3. Model results

3.1. Physical variables

The physical model produces good approximations to observed mixed layer depths (Figs. 4a and 5). The annual cycle of thermal mixing and stratification produced by the model (Fig. 6a) agrees well with trends reported for the region (Angel, 1984; Gardner et al., 1999). Stations A1 and A3 both exhibit strong stratification during the inter-monsoon periods, with pronounced mixing events associated with the SW monsoon and to a lesser extent the NE monsoon. During the monsoons, the base of the euphotic zone is in the mixed layer, whilst during the inter-monsoon periods it lies in the thermocline, consistent with Brock et al. (1993). The SWM Arabesque cruise coincides with a period of rapid decrease in simulated mixed layer depth at both stations A1 and A3. Relaxation after mixing events appears to be reasonably rapid. The INEM cruise coincides with the end of a fairly stable simulated thermal structure and the initial mixed layer deepening associated with the

Table 5
Phytoplankton model parameters

Description	Unit	Diatoms	Flagellates	Picoplankton	Dinoflagellates
Assimilation rate (10 °C)	day^{-1}	2.0	2.25	3.15	1.6
Basal respiration (10 °C)	day^{-1}	0.2	0.2	0.2	0.2
Exudation under nut. stress	–	0.05	0.10	0.15	0.05
Activity respiration	–	0.2	0.45	0.5	0.45
Redfield N/C ratio	mmol N $(mg C)^{-1}$	0.0126	0.0126	0.0126	0.0126
Minimal N/C ratio	mmol N $(mg C)^{-1}$	0.00687	0.00687	0.00687	0.00687
Maximum N/C ratio	mmol N $(mg C)^{-1}$	0.0252	0.0252	0.0252	0.0252
Redfield P/C ratio	mmol P $(mg C)^{-1}$	0.786e – 3	0.786e – 3	0.786e – 3	0.786e – 3
Minimal P/C ratio	mmol P $(mg C)^{-1}$	0.428e – 3	0.428e – 3	0.428e – 3	0.428e – 3
Maximum P/C ratio	mmol P $(mg C)^{-1}$	0.157e – 2	0.157e – 2	0.157e – 2	0.157e – 2
Affinity for NO_3	$(mg C)^{-1}$ day^{-1}	0.0025	0.0025	0.0025	0.0025
Affinity for NH_4	$(mg C)^{-1}$ day^{-1}	0.01	0.01	0.015	0.01
Affinity for PO_4	$(mg C)^{-1}$ day^{-1}	0.0025	0.0025	0.0025	0.0025
Nutrient stress threshold	–	0.70	0.75	0.75	0.75
Nutrient stress sedimentation rate	m day^{-1}	5.0	0.0	0.0	5.0
Minimal lysis rate	day^{-1}	0.05	0.05	0.05	0.05
Si uptake Michaelis constant	mmol Si m^{-3}	0.3	–	–	–
Standard Si/C ratio	mmol Si $(mg C)^{-1}$	0.03	–	–	–

Table 6
Zooplankton model parameters

Description	Unit	Heterotrophic flagellates	Microzooplankton	Mesozooplankton
Assimilation rate at 10 °C	day^{-1}	1.63	0.8	0.33
Food concentration where relative uptake is 0.5	mg C m^{-3}	120.0	80.0	40.0
Assimilation efficiency	–	0.4	0.5	0.6
Fraction of excretion going to DOM	–	0.5	0.5	0.5
Basal respiration rate at 10 °C	day^{-1}	0.02	0.02	0.02
Oxygen saturation where respiration is 0.5	mmol m^{-3}	7.8125	7.8125	7.8125
Excreted fraction of uptake	–	0.5	0.5	0.5
Mortality due to oxygen limitation	day^{-1}	0.25	0.25	0.25
Temperature independent mortality	day^{-1}	0.05	0.05	0.075
Max. quotum N/C	mmol N (mg C)$^{-1}$	0.0167	0.0167	
Max. quotum P/C	mmol P (mg C)$^{-1}$	0.001	0.001	
Lower threshold (mg C m^{-3}) for feeding	mg C m^{-3}	15.0	10.0	1.0
Damping coefficient in N-excr.	day^{-1}	0.5	0.5	
Damping coefficient in P-excr.	day^{-1}	0.5	0.5	

onset of the NEM. Annual cycles of mixed layer depth and euphotic depth for A3 closely match the mooring data for the similarly located US JGOFS mooring (Kinkade et al., 2001). Station A7 exhibits a deeper, essentially permanent thermal stratification in the absence of strong wind forcing.

3.2. Nutrients

The modelled nitrate cycle (Fig. 6b) and modelled profiles validated by measurements (Fig. 7) show a progressive deepening of the nutricline from North to South that is disturbed only by the monsoonal mixing events. At A1 modelled surface concentrations of nitrate exceed 5 mmol·m^{-3} during the SW monsoon, comparing well with observed values in the range 3–7 mmol·m^{-3} (Woodward et al., 1999). The position of the nutricline also agrees well with measurements (Fig. 7a). Modelled surface nitrate at A3 during the SWM cruise period are lower than measured, (<0.5 mmol m^{-3} c/w >5 mmol m^{-3}). During the inter-monsoons and at the permanently oligotrophic station A7, modelled surface levels of nitrate are extremely low and correspond very closely with measured values (<0.25 mmol m^{-3} at A1, <0.1 mmol·m^{-3} at A3 and A7), as do the nutricline depths as evidenced in Fig. 7d–f. Both modelled and observed N/P ratios are low (<10.0) indicating phosphate limitation is not a feature of the region.

Table 7
Feeding (preference) matrix

From	To		
	Heterotrophs	Microzoos	Mesozoos
Bacteria	1.0	0.5	–
Picophytoplankton	1.0	1.0	0.1
Flagellates	–	1.0	1.0
Diatoms	–	–	1.0
Dinoflagellates	–	–	1.0
Heterotrophic flagellates	0.2	1.0	0.5
Microzooplankton	–	0.2	1.0
Mesozooplankton	–	–	0.2

The range of ammonium as measured on the SWM cruise is well reproduced by the model, concentrations peak at 4.07 mmol·m^{-3} at A1, 1.52 mmol m^{-3} at A3 and 0.68 mmol m^{-3} at A7, comparing with measured peak values of 4.05, 1.91 and 0.74, respectively (Woodward et al., 1999). In contrast with measurements that show a more diffuse distribution in the surface mixed layer, albeit highly variable, modelled ammonium exhibits a sub-surface maxima at all stations, deepening progressively with distance from the Omani coast. Peak ammonium concentrations are typically found above the nitrate nutricline and just below the areas of peak phytoplankton concentration.

Modelled silicate profiles show good agreement with data at A1 and A7 with both surface mixed layer concentrations and nutricline depth corresponding to measurements (Woodward et al., 1999). A similar mismatch as observed with the nitrate is evident at A3, modelled surface layer silicate during the SWM

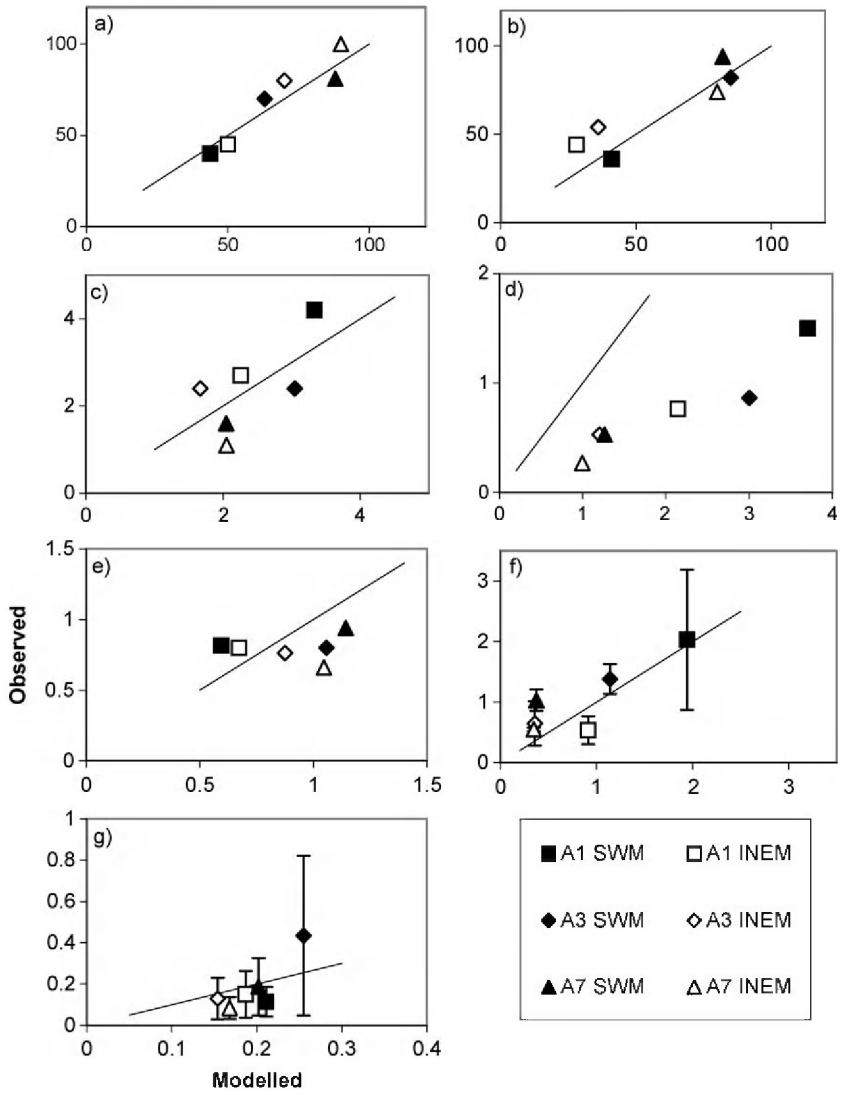

Fig. 4. Comparisons of model results with data from the Arabesque cruises; (a) 1% light depth (m), (b) mixed layer depth (m), (c) phytoplankton biomass (g C m^{-2}), (d) zooplankton biomass (g C m^{-2}), (e) bacterial biomass (g C m^{-2}), (f) primary production (g C m^{-2} d^{-1}), (g) bacterial production (g C m^{-2} day^{-1}). Modelled values are given on the *x*-axis, observations on the *y*-axis. The solid line represents 1:1 correspondence. The bars on (f) and (g) represent the range of measured data.

being too low (0.4 c/w 1.7 mmol m^{-3}) and nutricline depth too deep.

3.3. Primary producers

At each modelled station, inter-monsoonal periods are characterised by deep production/biomass maxima at 35 m (A1), 55 m (A3) and 75 m (A7), in reasonable agreement with observed deep chlorophyll maxima at 35, 60 and 70 m, respectively (Barlow et al., 1999; Savidge and Gilpin, 1999) (Fig. 8a). The biomass associated with the deep maxima decline with distance from the Omani coast, at the oligotrophic A7 being about one third that of the biomass at A1. Modelled monsoonal periods are characterised by surface blooms at A1 and A3. In agreement with data the

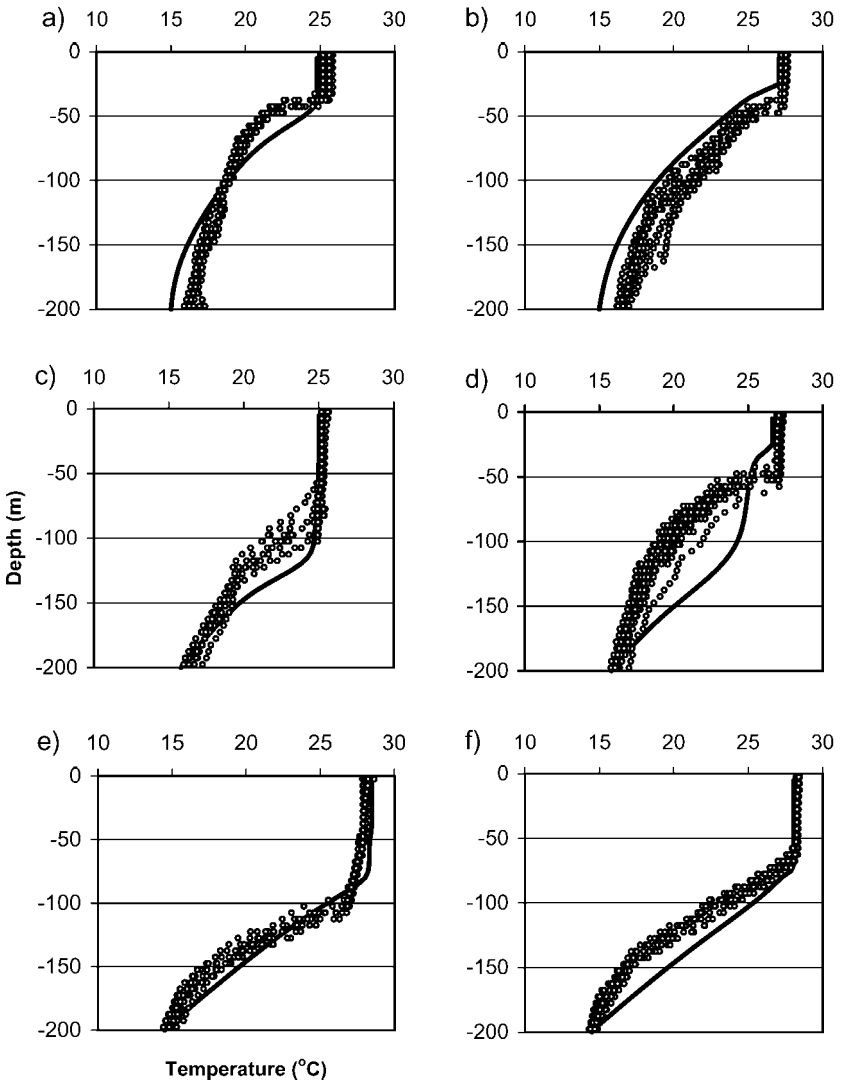

Fig. 5. Comparison of modelled (solid line) and measured (dots) temperature profiles for (a) station A1 during the SWM cruise; (b) A1, INEM cruise; (c) A3, SWM; (d) A3, INEM; (e) A7, SWM; (f) A7, INEM.

SW monsoonal bloom reaches deeper at A3 than at A1 in response to the deeper mixed layer and nutricline. Depth integrated phytoplankton biomass reaches 6.6 g C m^{-2} at A1 and 6.2 g C m^{-2} at A3 during the SW monsoon. Significant blooms are also simulated during the NE monsoon with peak phytoplankton biomass at 3.9 and 3.3 g C m^{-2} at A1 and A3, respectively. The A7 simulation exhibits a very weak surface bloom in response to mixing during the SWM period. Modelled depth integrated biomass during the intermonsoon periods show less of a spatial trend, the decline in concentration from the Omani coast being offset by the deepening of the euphotic zone. In comparison with data, the model appears to over-predict phytoplankton biomass at A7 during the INEM period, however the general seasonal and spatial trends measured during ARABESQUE are reproduced (Fig. 4c).

At A1 modelled primary production (Fig. 9) during the SW monsoon agrees closely with that measured during the ARABESQUE cruise (Savidge and Gilpin,

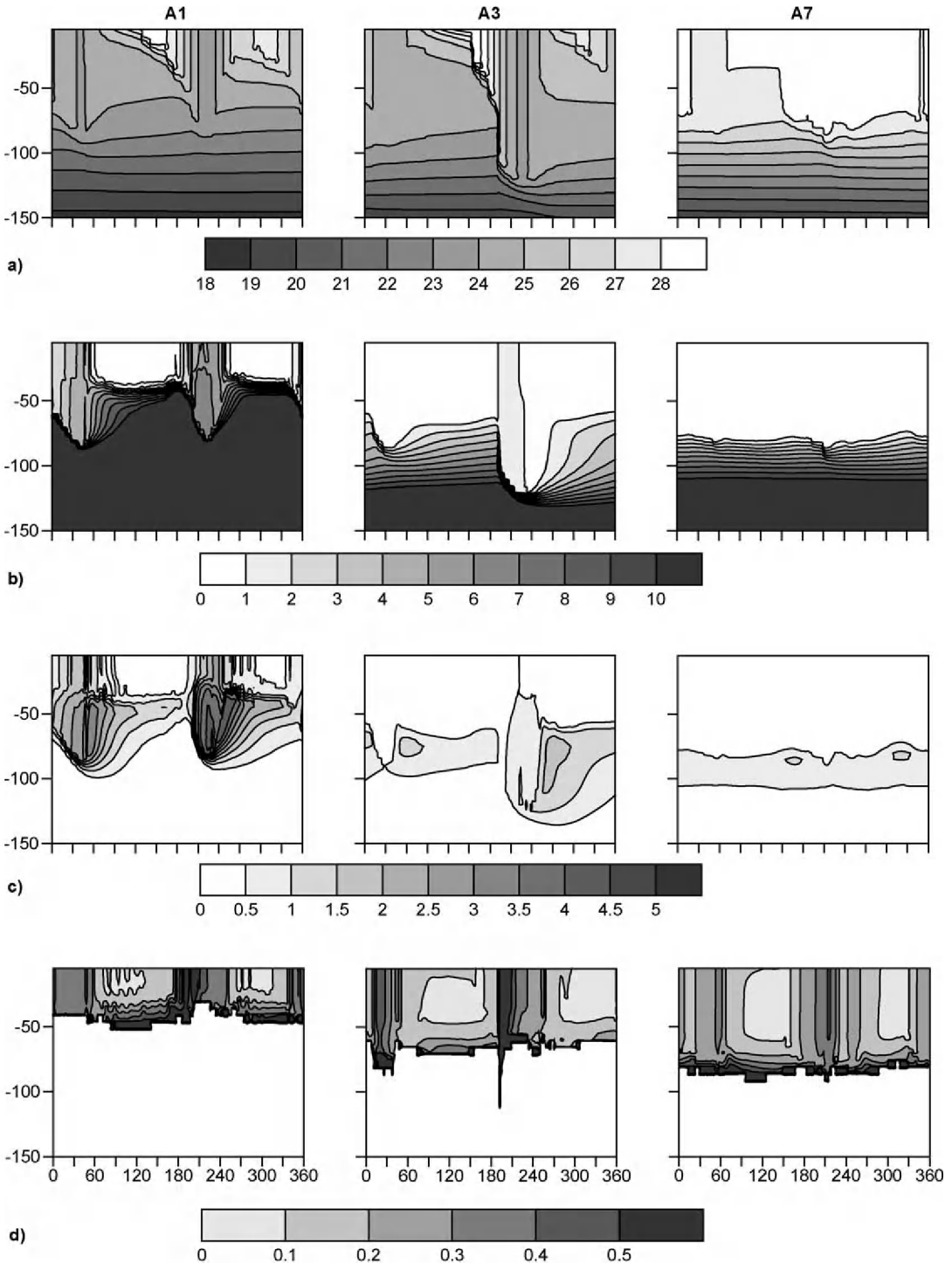

Fig. 6. Annual cycle of (a) temperature (°C); (b) nitrate (mmol N m^{-3}); (c) Ammonium (mmol N m^{-3}) and (d) *f*-ratio for the top 150 m for each station.

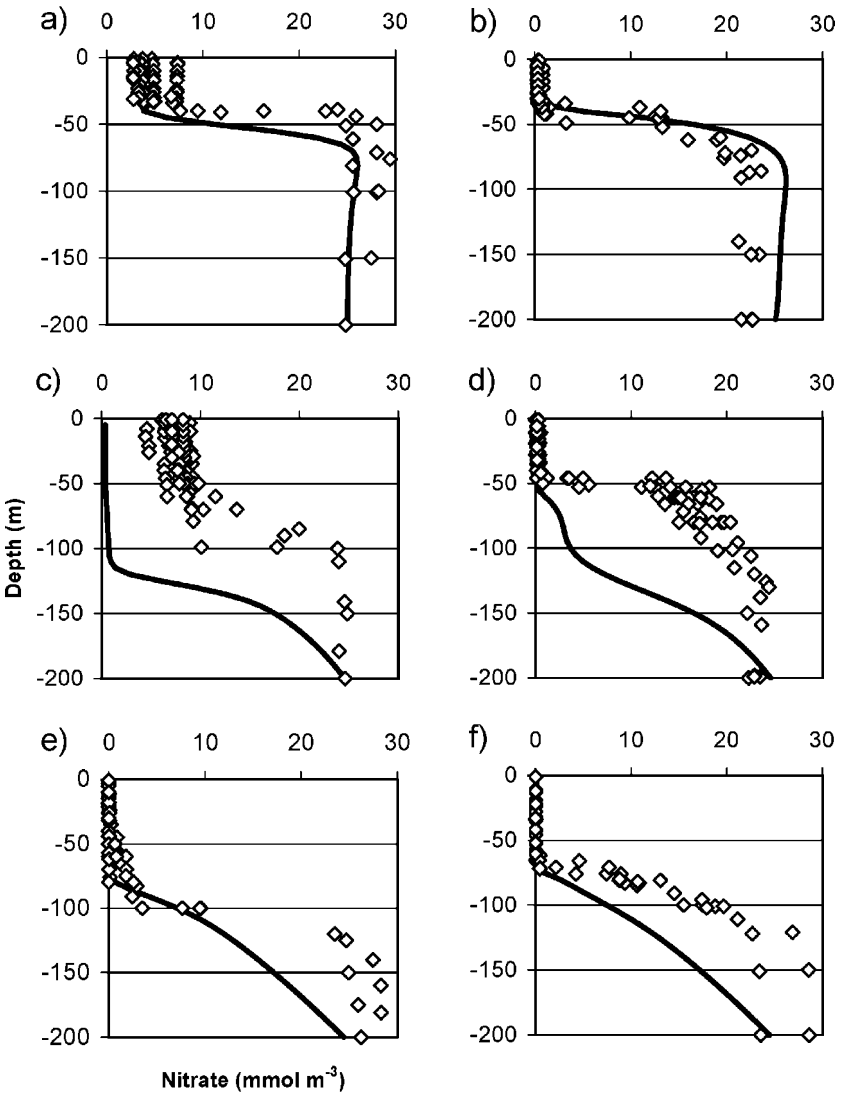

Fig. 7. Comparison of modelled (solid line) and measured (diamonds) nitrate profiles for (a) station A1 during the SWM cruise; (b) A1, INEM cruise; (c) A3, SWM; (d) A3, INEM; (e) A7, SWM; (f) A7, INEM, (mmol N m^{-3}).

1999), but is slightly higher than that measured on similar stations during the US JGOFS program (Barber et al., 2001). Conversely modelled production at A1 during the remainder of the annual cycle agrees well with Barber et al. (2001) but slightly over estimates ARABESQUE measurements for the INEM period. Modelled production at A3 is consistently lower than both UK and US data, consistent with the under estimation of nutrients in the model, although the seasonal signal seems qualitatively correct.

Depth integrated *f*-ratios (Fig. 6d) are generally low in all simulations, with annual means of 0.35, 0.24 and 0.24 for stations A1, A3 and A7, respectively. Season minima are associated with inter-monsoon periods (0.28, 0.11 and 0.13, respectively) and maxima with the monsoon events (0.65, 0.89 and 0.41, respectively). Locally, high *f*-ratios (>0.5) are associated with the base of deep chlorophyll maxima at all stations, where production is driven by the nutricline. Model results agree well with measurements by Watts and

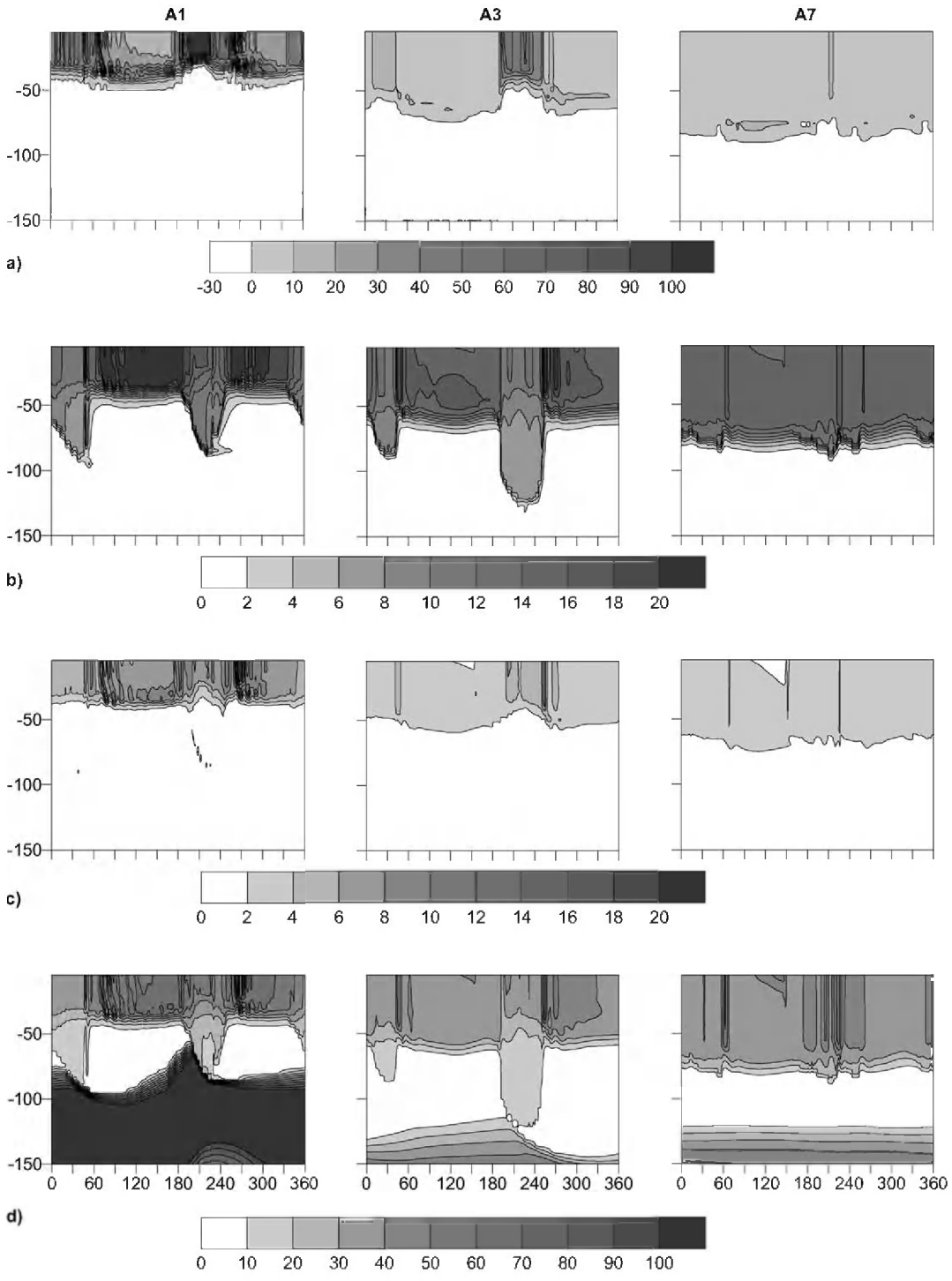

Fig. 8. Annual cycle of (a) primary production (mg C m^{-3} day^{-1}); (b) bacterial biomass (mg C m^{-3}); (c) bacterial production (mg C m^{-3} day^{-1}) and (d) total dissolved organic carbon (mg C m^{-3}), for the top 150 m for each station.

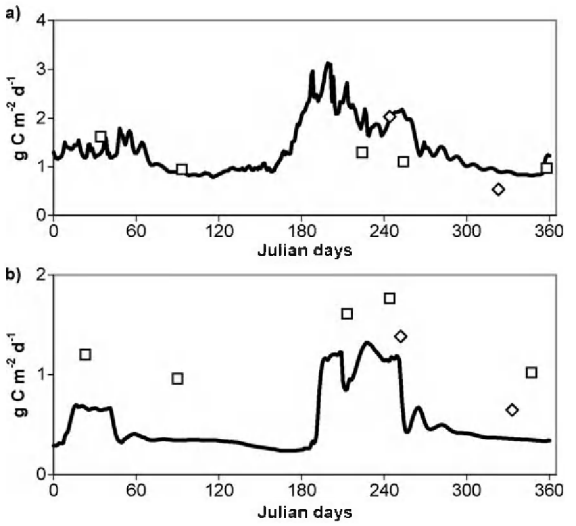

Fig. 9. Modelled annual cycles of primary production (solid line) for (a) station A1 and (b) station A3, compared with data from the ARABESQUE (◇) and US JGOFS (□) studies. US JOGFS station S07 corresponds exactly with ARABESQUE station A3, The mean of US JGOFS stations S02 and S03 has been used to compare with ARABESQUE station A1.

Owens (1999) who recorded *f*-ratios of 0.33, 0.24 and 0.21 (at stations A1, A3 and A7, respectively) during the INEM cruise.

3.4. Bacteria and DOM

The model predicts that the semi-labile dissolved pool, contributes 69%, 89% and 90% (for stations A1, A3 and A7, respectively) to the total organic carbon content, integrated over the 200 m depth range of the simulations. The labile dissolved pool contributes 15%, 5% and 6%, respectively with particulates accounting for 10%, 5% and 4%, respectively. However the majority of labile DOC exists below the photic zone (Fig. 8d), in areas of low oxygen concentration where degradation by aerobic bacteria is minimal. In the well-oxygenated mixed layer, concentrations of labile DOC average about 40 mg C m^{-3}, with peaks (60–80 mg C m^{-3}) associated with the end of monsoon periods. Labile DOC remains slightly elevated during the inter-monsoon at A1 (50 mg C m^{-3}). The model predicts a significant pool of semi-labile DOC which acts as a carbon cycle buffer as hypothesized by Azam et al. (1994) and reported by Ducklow et al. (2001), although surface DOC in the model (labile + semi-labile) ranges from 800 to 2300 mg C m^{-3} compared with cruise mean measurements of 888–984 mg C m^{-3}. Certainly the basic assumption that half of produced DOC is labile, half semi-labile is open to question, although the lack of advective loss terms may also explain DOC build up in the model water columns.

Measured total organic carbon (Hansell and Peltzer, 1998), from the US JGOFS transect, show an increase with distance from the Omani coast of about 1.0 mol C m^{-2} and a seasonal decrease after the SW monsoon of ~ 2.0 mol C m^{-2}. The model replicates these trends, producing a mean increase of ~ 3.0 mol C m^{-2} with distance from Oman and a post monsoonal decrease of ~ 2.6 mol C m^{-2}. The discrepancy in spatial trend may be due to the fact that the US JGOFS transect did not reach as far into the oligotrophic region as the Arabesque cruises. Both model and data also show a vertical decrease in TOC, although the modelled profiles (1.5–2.0 g C m^{-3} surface, < 0.1 g C m^{-3} at 150 m) are more exaggerated than the measured data (0.9 g C m^{-3} surface, 0.5 g C m^{-3} at 150 m).

Modelled estimates of bacterial biomass and production are in reasonable agreement with data (Pomroy and Joint, 1999; Wiebinga et al., 1997; Fig. 4e and g). Modelled bacterial biomass shows a small increase with distance from the Omani coast (0.7, 0.95 and 1.1 g C m^{-2} at A1, A3 and A7, respectively) not supported by measurements, but show little of the seasonality and spatial patterns exhibited by the autotrophs. Ducklow et al. (2001) found that bacterial production was suppressed during the NE monsoon and early SW monsoon and slightly elevated during the spring inter-monsoon, features that the model reproduces. A maximum seasonal signal of ~ 1.7 fold increase over the SW monsoon also agrees well with the maximum < 2 fold increase observed by Ducklow et al. (2001). Modelled net bacterial production is slightly higher at A1 (206 mg C m^{-2} day^{-1}) than at A3 or A7 (161 and 178 mg C m^{-2} day^{-1}). It is notable that bacterial production at A3 during the SWM cruise period is consistently high in both model and data. In the model, this is due to a short-lived but significant peak in DOC production at the end of the monsoon period as nutrient-stressed cells undergo lysis. This feature is also simulated at A1, but does not coincide with the cruise.

3.5. Zooplankton

Modelled total zooplankton biomass (mesozooplankton, microzooplankton and heterotrophic nanoflagellates; Fig. 10) generally follows the pattern of phytoplankton biomass, peaking 10–30 days after monsoon phytoplankton blooms. The percentage of zooplankton within total plankton decreases with distance from the Omani coast, being on average 43% at A1, 32% at A3 and 26% at A7, as does the mean zooplankton biomass, 2783, 1553 and 1151 mg C m^{-2}, respectively (Table 8). During the later stages of both monsoons, at A1 and A3, zooplankton standing stocks exceed that of phytoplankton. In contrast with the picoplankton dominated phytoplankton, zooplankton are dominated throughout the annual cycle by the larger mesozooplankton class at station A1. This supports observations that the microbial loop is an important source of food for zooplankton during the inter-monsoon (Madhupratap and Gopalakrishnan, 1996). At A3 the zooplankton are a more mixed community and whilst mesozooplankton are still the largest group by biomass, both heterotrophic flagellates and microzooplankton are significant. At A7

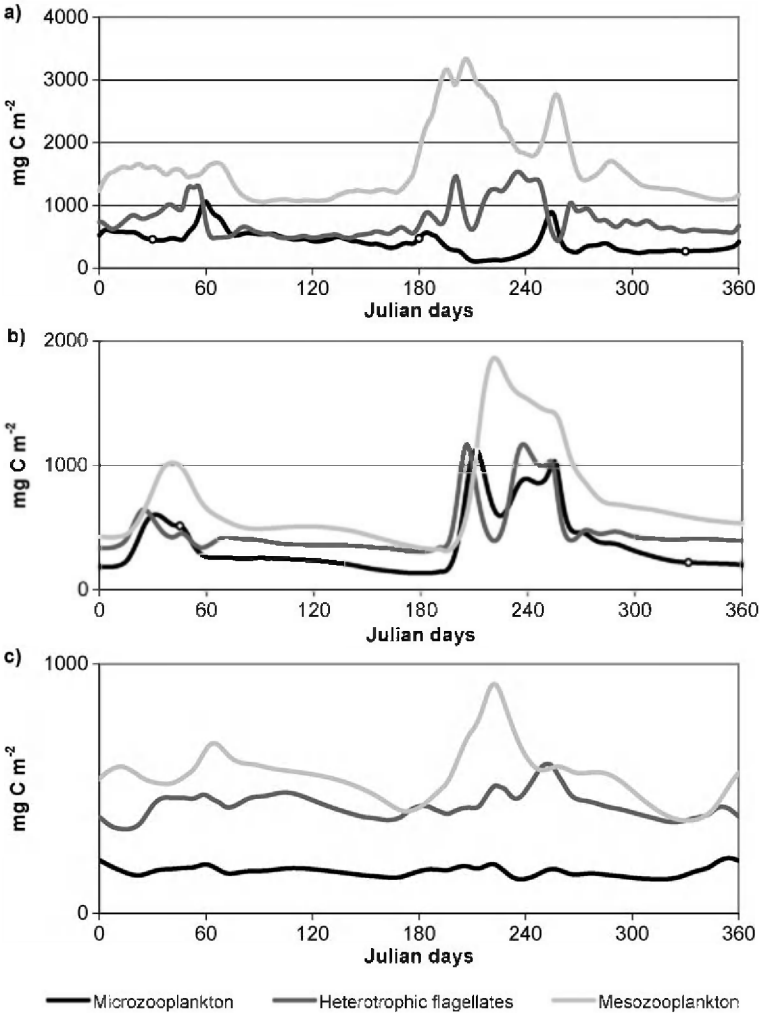

Fig. 10. Depth integrated annual cycles for the zooplankton community: (a) station A1, (b) A3, (c) A7, (mg C m^{-2}).

Table 8
Annual mean biomass and community structure for each modelled station

Station		A1	A3	A7
Total biomass (mg C m^{-2})		6521	4889	4348
% Contribution to biomass total	Phytoplankton	46	49	48
	Zooplankton	43	32	26
	Bacteria	11	19	26
% Contribution to phytoplankton total	Diatoms	22	9	7
	Flagellates	16	22	23
	Picoplankton	58	60	53
	Dinoflagellates	4	9	18
% Contribution to zooplankton total	Heterotrophic flagellates	27	30	37
	Microzooplankton	15	24	15
	Mesozooplankton	58	46	48

heterotrophic flagellates join mesozooplankton as the dominant grazers by biomass. The model reproduces the measured spatial and seasonal trends (Stelfox et al., 1999) although zooplankton biomass is consistently over estimated, in comparison with the ARABESQUE data, by a factor of 2.85 ± 0.5. However other surveys (e.g. Sorokin et al., 1985; Reckermann, 1996; Smith et al., 1998b; Roman et al., 2000) have recorded higher zooplankton standing stocks in the region that correspond closely with modelled values. For example Roman et al. (2000) measured an inshore–offshore biomass range of ~ 1.2 to 0.5 mg C m^{-2} during the inter-monsoon and ~ 3.2 to 0.75 during the late SW monsoon. The range of model results is respectively 1.1–0.5 and 3.3–0.9 mg C m^{-2}.

Modelled bactivory is higher in upwelling systems throughout the year, showing sustained levels around 150 mg C m^{-2} day^{-1} during the intermonsoon and a decline during the monsoon periods. Short-lived peaks in bactivory (>300 mg C m^{-2} day^{-1}) are predicted at the end of both monsoons. Bactivory at the oligotrophic station is constant at around 100 mg C m^{-2} day^{-1}. Bactivory by heterotrophic nanoflagellates dominates that of microzooplankton throughout the annual cycles. These results are consistent with observations of hourly bacterial grazing rates (Weisse, 1999).

Estimates of mesozooplankton herbivory derived from the ARABESQUE transect are very variable, ranging from 3–64 mg C m^{-2} day^{-1} at A7 during the intermonsoon to 24–204 mg C m^{-2} day^{-1} at A1 during the SWM cruise. Modelled mesozooplankton herbivory shows good agreement to the spatial and seasonal trend measured, with herbivory of ~ 100 mg C m^{-2} day^{-1} at A7 during the intermonsoon and ~ 680 mg C m^{-2} day^{-1} at A1 during the SW monsoon. Applying the same factor derived from the differences between measured and modelled zooplankton biomass, modelled herbivory is consistent with estimates of herbivory from the field. Mesozooplankton ingestion measured on the US JGOFS transect (Roman et al., 2000), whilst also variable, compare well with those modelled (Table 9). Microzooplankton herbivory of 29–496 mg C m^{-2} day^{-1} accord well with measurements by Edwards et al. (1999) of 161–300 mg C m^{-2} day^{-1}. Estimations of microzooplankton herbivory in the north east of the region during the NE monsoon (Reckermann and Veldhuis, 1997) of 38% of total phytoplankton biomass, 67% of total production, 49% of picophytoplankton biomass and 102% of picophytoplankton production compare with model results of 28%, 67%, 42% and 100%, respectively.

3.6. Modelled plankton community structure

From the perspective of annual means (Table 8), within the trend of decreased plankton biomass with distance from the Omani coast, the contribution of phytoplankton to total biomass remains constant at just under 50%. Zooplankton, from been almost on a par with phytoplankton at A1 (43%) decreases to 26% of the total at A7, whilst bacteria shows the reverse trend, increasing from 11% at A1 to 26% at A7. This compares with ranges of 43–64% for phytoplankton and 16–44% for bacteria recorded on the US JGOFS transect (Garrison et al., 2000).

Table 9
Mesozooplankton ingestion rates (mg C m^{-2} day^{-1}) from the model and the US JGOFS process study

Period	S02 Data	A1 Model	S07 Data	A3 Model
Late NE monsoon	390	431	139	154
Spring inter-monsoon	456	318	702	98
Late SW monsoon	527	628	349	344
Early NE monsoon	708	371	606	110

Modelled station A3 is compared with the co-incident US station S07, modeled station A1 is compared with the nearby US station S02. The Hirst–Sheader estimates from Roman et al. (2000) are used.

The composition of the phytoplankton community shows distinct spatial and temporal trends (Fig. 11). Generally picophytoplankton are the dominant functional group, in agreement with observations (Tarran et al., 1999), contributing 50–60% of inter-monsoonal phytoplankton biomass and up to 90% during the monsoonal community succession. Diatoms, flagellates and picophytoplankton are associated with monsoonal forcing whilst the dinoflagellates are generally absent from monsoonal periods. Diatoms only contribute significantly during periods of monsoonal forcing when they can account for over 70% of phytoplankton biomass, again reflecting observations, e.g. Garrison et al. (2000) and Tarran et al. (1999).

At station A1 the four phytoplankton classes exhibit contrasting behaviour throughout the annual cycle (Fig. 11a). Competition between diatoms and dinoflagellates, which otherwise have a similar model niche depends on the availability of silicate. Hence diatoms are predicted only in a narrow band in the vicinity of the nutricline during inter-monsoon periods and distributed throughout the mixed layer during the monsoon seasons, the *f*-ratio for diatoms being consistently greater than 0.4. The distribution of the dinoflagellates is restricted to the remaining parts of the photic zone where they are predominantly dependent on recycled nutrients (*f*-ratio ~ 0.2). Picophytoplankton and flagellates show similar distributions during intermonsoon periods, associating with both the nutricline and nutrient recycling (*f*-ratios = 0.2–0.4). For all functional groups, competition and seasonal succession is enhanced during the monsoon bloom period with diatoms and picophytoplankton showing oscillating negatively correlated distributions. Towards the end of the SW monsoon, when the mesozooplankton grazers are dominant, carnivory of the micro-grazers provides a niche for a flagellate bloom.

Although the gross community structure at A3 is similar to that at A1, certain differences are evident. At A3 (Fig. 11b), diatoms are much more restricted than at A1 occurring only during the late SW monsoon (*f*-ratios>0.4). Dinoflagellates replace diatoms for all but the SW monsoon period. Flagellates exploit the late development of diatoms, showing higher monsoonal densities than at A1.

Two distinct communities appear to exist at A7 (Fig. 11c), a mixed layer community of flagellates and dinoflagellates deriving nutrients from recycling (*f*-ratios ~ 0.2) and a diatom (*f*-ratio ~ 0.5) and picophytoplankton community (*f*-ratio ~ 0.3) associated with the sub-surface maxima and dependant more on new production. This accords well with observations by Jochem et al. (1993).

The annual mean ratio of bacterial production (BP) to primary production (PP) increases with distance from the Omani Coast (0.17 at A1, 0.38 at A3 and 0.49 at A7). Plots of bacterial production against primary production for the spring inter-monsoon, SW and NE monsoon periods (Fig. 12a) show a number of distinct regimes, replicated by similar plots of bacterial biomass to phytoplankton biomass (Fig. 12b). During inter-monsoon periods at A3 and A7 bacterial and primary production appear to be strongly coupled and BP/PP ratios are about 0.45. This direct coupling is not evident during the inter-monsoon at A1, when the BP/PP ratio is ~ 0.2. Although the BP/PP ratio during monsoon periods at A1 and A3 exhibits similar values (~ 0.1), A3 tends to exhibit a smoother relationship, whilst at A1 the relationship is far more chaotic. At A7 during the SW monsoon, although the BP/PP ratio remains at similar levels to the intermonsoon period, the direct coupling has ceased and perturbation is evident. Analysing biomass to production ratios for both bacteria and phytoplankton indicates that A1 is characterized by high ratios throughout the annual cycle (~ 0.43 for phytoplankton) whilst the ratio at A3 and A7 is consistently lower (~ 0.17). Hence grazing is far more important at A1 (grazing amounting to 20–40% per day) than at the other stations (grazing ≤ 15% per day) and is evidenced by a more chaotic relationship between bacteria and phytoplankton. On the other hand, the monsoonal periods are characterized by mixing induced perturbations, shifting the size structure of the phytoplankton community and the response time of the grazing community. The modelled NE monsoon is seen to be far less dynamic, exhibiting relatively little perturbation in bacterial or phytoplanktonic response. During the intermonsoon periods at A3 and A7, the coupling between bacterial and phytoplankton populations is initially due to bacterial dependence on DOC production by phytoplankton and latterly direct bacterial competition for nutrients with the phytoplankton.

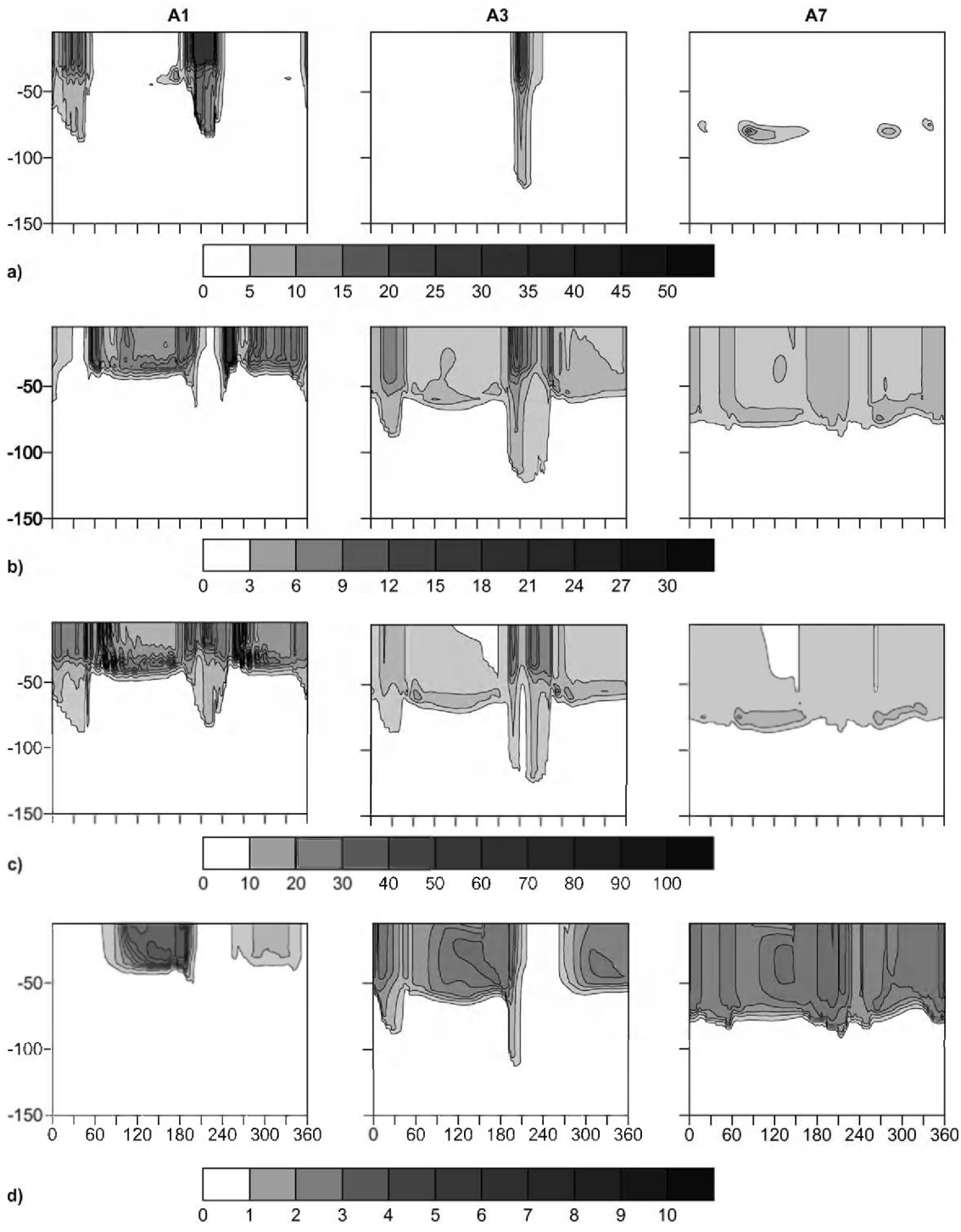

Fig. 11. Annual cycles of the phytoplankton functional groups at each station (a) diatoms, (b) flagellates, (c) picoplankton, (d) dinoflagellates (mg C m^{-3}).

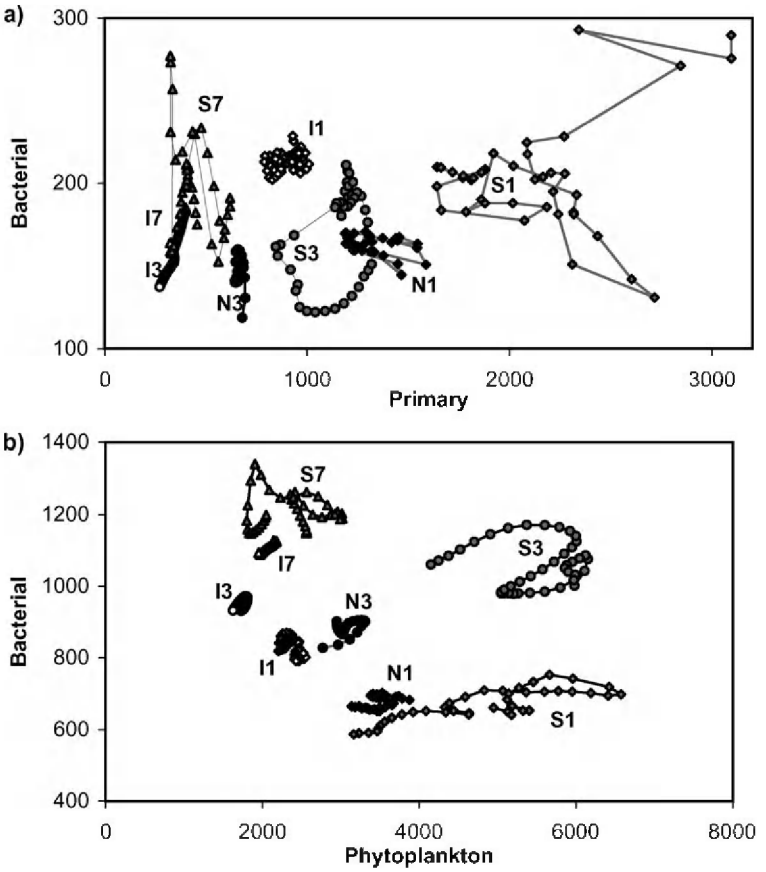

Fig. 12. (a) Bacterial against primary production (mg C m^{-2} day^{-1}) and (b) bacterial against phytoplankton biomass (mg C m^{-2}) for three contrasting periods. The spring intermonsoon (Julian days 90–150), denoted by I, the SW monsoon (Julian days 200–240), denoted by S and the NE monsoon (Julian days 15–45), denoted by N for each modelled station, (A)1, (A)3 and (A)7. The NE monsoon for A7 is not shown as it coincides with the inter-monsoon at A7.

3.7. Fluxes

Table 10 gives the modeled annual mean carbon fluxes between key functional groups for each station. Net CO_2 uptake by the primary producers shows little spatial variation between each station with fluxes through picophytoplankton dominating, in agreement with Savidge and Gilpin (1999) and Barber et al. (2001). A shift away from diatoms and towards smaller size classes with distance from the Omani coast is also produced by the model agreeing with observations by Latasa and Bidigare (1998) and Barlow et al. (1999). The fate of assimilated CO_2 does however show marked spatial variation with POC and DOC production, generally via nutrient stress induced lysis, accounting for 58% of net production at A1 but 84% at A3 and 92% at A7. In contrast grazing is significantly greater at A1 than A3 and, in turn, A7, with herbivory accounting for 39%, 15% and 8% of net CO_2 uptake, respectively, and carnivory accounting for 38%, 31% and 25% of secondary production, respectively.

Table 11 illustrates the same carbon fluxes for different seasons and monsoonal sub-seasons at station A1. Primary production by the small picophytoplankton class dominates throughout. Diatom production peaks are associated with both the NEM and SWM. Diatom lysis reaches a maximum in early August. Peak herbivory and carnivory is associated with the SW monsoon. Grazing is the most variable component

Table 10
Annual mean carbon fluxes (mg C m^{-2} day^{-1}), for each modelled station

	A1	A3	A7
Net phytoplankton CO_2 uptake			
by Picophytoplankton	2106	1783	1932
by Flagellates	385	402	544
by Diatoms	366	83	62
by Dinoflagellates	49	103	213
Total net CO_2 uptake	2906	2371	2751
Excretion/lysis to DOC/POC			
by Picophytoplankton	1304	1522	1802
by Flagellates	200	327	495
by Diatoms	174	64	53
by Dinoflagellates	23	83	181
by Heterotrophic flagellates	259	96	77
by Microzooplankton	103	58	23
by Mesozooplankton	387	100	69
Total phytoplankton loss	1701	1996	2531
Total consumer loss	749	254	169
by Bacteria	43	58	73
Bacterial production			
Bacteria	1974	2291	2804
Herbivory			
by Heterotrophic flagellates	553	153	90
by Microzooplankton	232	114	38
by Mesozooplankton	347	92	83
Total herbivory	1132	359	211
Bactivory			
of Bacteria	159	103	106
Carnivory			
by Heterotrophic flagellates	40	6	4
by Microzooplankton	67	22	7
by Mesozooplankton	321	82	42
Total carnivory	428	110	53
Respiration			
by Bacteria	1725	2072	2553
by grazers	578	225	158
System budget			
Sedimentation	198	54	36
Loss of CO_2 to Atmospheric	62	−13	−8
Net community CO_2 uptake	603	74	40

of the system, whilst the microbial loop and the associated remineralisation the least variable.

Significant annual plankton community fixation of CO_2 is only evident at A1 (216 g C m^{-2} $year^{-1}$), photosynthesis and respiration at stations A1 and A3 are more balanced (26 and 14 g C m^{-2} $year^{-1}$ net fixation respectively). Despite the higher fixation, significant CO_2 out-gassing is indicated at station A1

Table 11
Seasonal carbon fluxes at station A1 (mg C m^{-2} day^{-1})

	NEM	SIM	SWM		AIM
	345-70	71-150	151-210	210-270	271-345
Net phytoplankton CO_2 uptake					
by Picophytoplankton	1845	2294	2193	2339	1939
by Flagellates	264	403	376	452	456
by Diatoms	285	87	971	561	124
by Dinoflagellates	11	112	59	96	45
Total net CO_2 uptake	2405	2896	3599	3448	2564
Excretion/lysis to DOC/POC					
by Picophytoplankton	967	1739	1273	1190	1315
by Flagellates	112	275	186	162	259
by Diatoms	156	50	401	284	60
by Dinoflagellates	5	50	30	3	15
by Heterotrophic flagellates	252	161	287	418	228
by Microzooplankton	132	111	100	93	73
by Mesozooplankton	322	242	563	586	310
Total phytoplankton loss	1240	2114	1890	1639	1649
Total consumer loss	706	514	950	1097	611
by Bacteria	41	50	43	39	42
Bacterial production					
Bacteria	1802	2231	2024	1895	1910
Herbivory					
by Heterotrophic flagellates	565	307	623	923	462
by Microzooplankton	301	245	225	222	161
by Mesozooplankton	241	173	664	523	256
Total herbivory	1107	725	1512	1668	879
Bactivory					
of Bacteria	131	161	174	174	161
Carnivory					
by Heterotrophic flagellates	33	14	41	86	36
by Microzooplankton	87	59	67	68	52
by Mesozooplankton	300	230	588	466	272
Total carnivory	420	303	696	620	360
Respiration					
by Bacteria	1585	1966	1751	641	1665
by grazers	570	411	704	815	481
System budget					
Sedimentation	150	152	158	341	212
Loss of CO_2 to Atmospheric	9	−12	193	213	−27
Net community CO_2 uptake	250	517	1144	904	417

during the SW monsoon (Fig. 13) when daily loss rates of CO_2 can exceed 0.5 g C m^{-2} day^{-1}. At this time-modelled values of pCO_2 agree well with measurements of Goyet et al. (1998). Annually a flux of 22 g C m^{-2} to the atmosphere is predicted, whilst small draw downs of CO_2 at A3 (5 g C m^{-2}) and A7 (3 g C m^{-2}) are simulated, in contrast to the generally predicted net regional outgassing throughout the region (Goyet et al., 1998; Körtzinger et al., 1997).

Sedimentation loss, measured at 200 m lags the peak in production by a few weeks (Fig. 13), and over the annual cycle is amounts to ~ 15% of net production at each station. Of total community CO_2 uptake, sedimentation accounts for 33% at A1 and 90% at A3 and A7. At the latter two stations, the remaining community uptake is accounted for by a build up of organic carbon, which in reality may be advected away. At A1, horizontal advection loss generated by the modelled upwelling accounts for the difference between community uptake and sedimentation. Plausibly the mass advected out of the water column would be subject to sedimentation downstream. Sedimentation rates are seen to be most closely associated with larger cell production or the classical foodweb (diatoms and mesozooplankton), with sedimentation events lagging 15–30 days behind production peaks, agreeing with the analysis of Rixen et al. (2000). A maximum simulated rate of ~ 400 mg C m^{-2} day^{-1} or approximately 20% of primary production at A1 agrees very well with measurements of ~ 300 and 17–28% for the late South West Monsoon (Buesseler et al., 1998). Honjo et al. (1999) observed a double maxima in sedimentation patterns during both the late South West and North East Monsoons, which is reproduced for the SWM in the model. The first maximum is associated with the diatom/meso-grazers

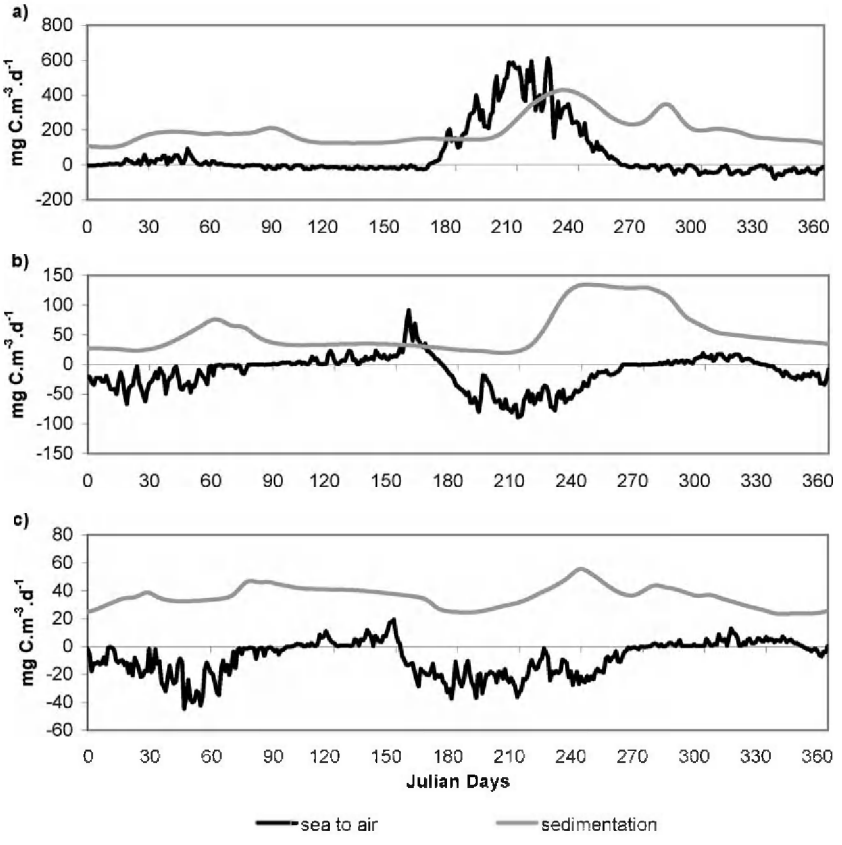

Fig. 13. Annual cycles of sedimentation loss (mg C m^{-2} day^{-1}) and CO_2 flux to the atmosphere (mg C m^{-2} day^{-1}) for (a) station A1, (b) A3 and (c) A7.

peak around Julian day 230, whilst the second is a product of a subsequent flagellate/meso-grazer peak at day 280. Modelled sedimentation rates for the NE Monsoon are in the order of half the magnitude of SW monsoon events, again in accordance with data (Honjo et al., 1999). Monsoon sedimentation peaks are predicted to consist predominantly of mesozooplankton fecal pellets, rather than ungrazed diatoms. Microbial food webs, dominant during the inter-monsoon periods and at the permanently oligotrophic stations, contribute little to sedimentation loss, averaging about 25 mg C m^{-2} day^{-1}, agreeing well with measurements of 22 mg C m^{-2} day^{-1} (Pollehne et al., 1993).

Grazer-autotroph oscillations are clearly seen in the net community CO_2 uptake, in association with the latter part of the monsoonal periods. All simulations indicate periods of net community CO_2 production that may indicate periods of grazer control.

4. Discussion

Despite the one-dimensional physical aspects of the coupled model, the simulations generate a high proportion of observed features in the region. A clear distinction between monsoonal and inter-monsoonal systems is shown and further distinctions between the North East and South West monsoons are clear. Trends of increasing oligotrophy away from the Omani coast are also reproduced. State variables and process rates generally validate well. Thus, if a reasonable approximation to upwelling is parameterised, then the state and rate variable dynamics are reproducible by considering water column processes only. Given that the simulations differ only in wind forcing, cloud cover, irradiance, background sediment loads, surface salinity and lower boundary temperature then one can infer that the local physical forcing alone can explain much of the complex spatial trends found in the region, in accordance with Fischer (2000).

The biggest errors in the model simulations occur at station A3. This could be a simple error in timing in the model, however the peak modelled surface nitrate during the SWM at A3 is only 1.7 mmol m^{-3} compared with observations of the order of 5 mmol m^{-3}, suggesting that a more fundamental process is missing from the A3 simulation. This is also evidenced by the profile mismatch for SWM nitrate at A3 (Fig. 7c–d) which shows the modelled nutricline to be too diffuse and too deep. It seems likely that the model's failure to inject sufficient nutrients into the photic zone is the root cause of the production shortfall at A3. Although not in the area generally thought to experience upwelling, a possibility is that the station was affected by an upwelling eddy, the US studies have shown filaments in this region (Dickey et al., 1998). Potentially the simulation of entrainment driven mixing is not sufficient to inject the observed quantities of nutrients to the surface layer. Lee et al. (2000) found that entrainment is at least seasonally important. One conclusion is that resolution to diurnal radiation forcing would be a valuable addition to the model (McCreary et al., 2001).

The model supports the findings of Savidge and Gilpin (1999) and Jochem et al. (1993) demonstrating the potential for significant primary production in the oligotrophic regions of the Arabian Sea. Under-estimates of primary production in the model may be due to the relatively high parameterisation of respiration used, but the modelled production underpins the dynamics of the microbial loop, which shows good agreements with data. Evidence of higher than assumed respiration rates in the region is given by Robinson and Williams (1999). Furthermore Dickson et al. (2001) found that stations with higher net production to gross production ratios also had higher DOC production rates compared to community respiration, a feature that the model reproduces. Presumably regions that respire less of the gross production produce cells with higher C/N ratios that are more prone to nutrient stress lysis and increased DOC production. This is certainly an important dynamic in the ERSEM model as a consequence of the Droop kinetics used to simulate nutrient limitation in phytoplankton. Lysis induced by low internal cell nutrient quotas can produce cell mortality rates of 10–50% day^{-1}. However model simulations using external nutrient concentrations to limit production show serious inconsistencies with measured data. Better estimates of respiration and DOC production rates are undoubtedly required.

Model results suggest that up to 90% of organic carbon in the upper Arabian Sea exist as DOC. The principle source of DOC is identified as nutrient stress lysis of phytoplankton. Two DOC maxima exist, one in surface waters, the other, significantly larger, below

the photic zone, impinging on the oxygen minimum zone characteristic of some Arabian Sea regions. This build up of sub-surface DOC in the model is due to mixing down and subsequent lack of advective lateral transport and possibly anaerobic decomposers. However, it is indicative of an important sink of organic carbon and concurs with observed accumulations of DOC in productive systems (Copin-Montegut and Avril, 1993; Carlson et al., 1994; Williams, 1995). Degradation of surface DOC in the model is restricted because bacterial growth rate is limited by competition for nutrients and to some extent bacterial biomass is controlled by predators, as demonstrated in a modelling context by Thingstad et al. (1997). Unlike most other system components, which decline towards the central Arabian Sea, neither bacteria nor mixed layer DOC show a pronounced spatial trend. Whilst bacteria become more nutrient constrained in oligotrophic waters, increased respiration, with increased temperature, offsets internal nutrient depletion and grazing pressure declines. Accumulation of DOC in surface layers may act to moderate the response of bacteria to temporal trends in production (Azam et al., 1994). This combination of factors may account for constant bacterial populations.

The model supports findings that the non-monsoonal Arabian Sea can generally be characterised as one in which small celled phytoplankton communities dominate (Tarran et al., 1999; Jochem et al., 1993; Burkill et al., 1993b). The model suggests that 80–95% of production is converted to DOC via cell lysis, providing a substrate for the microbial loop. Without perturbation, as evidenced by relatively constant bacterial production to primary production ratios, a multivorous grazing community develops, heterotrophic nanoflagellates grazing on picophytoplankton and bacteria with mesozooplankton grazing the larger phytoplankton cells and other zooplankton. The bulk of these dynamics are associated with sub-surface maxima with a combination of light and nutrients controlling the system.

The two monsoonal events that affect the North West of the region provoke complex spatial-temporal changes in the modelled planktonic community structure. The initial response to the SW monsoon at A1 are concurrent blooms of diatoms, flagellates and picophytoplankton driven by new production. The subsequent development of an omnivorous grazing community acts to suppress flagellates and causes predator prey oscillations alternately favouring diatoms and picophytoplankton. Towards the end of the monsoon, grazing pressure on diatoms and picophytoplankton creates a niche for flagellates that exploit the remaining now mainly recycled nutrients in the surface mixed layer. Similar patterns are modelled during the NE monsoon at A1 and both monsoons at A3, although blooms associated with the NE monsoon are dominated by the <2.0 and <20.0 phytoplankton size classes. The weaker mixing during the NE monsoon tends to favour the non-siliceous phytoplankton groups. This is consistent with theories that silica availability and hence diatom growth in the region is largely driven by strong coastal upwelling as a consequence of SW monsoonal forcing (Young and Kindle, 1994). Low *f*-ratios throughout the region indicate that the remaining phytoplankton communities are frequently dependent on recycled nutrients. Thus where upwelling is weak or non-existent diatoms are out competed. The model reproduces the strong observed coupling between monsoons, classical food webs and sedimentation (Garrison et al., 2000).

The model system used does not include a precise formulation of CO_2 partial pressure and subsequent air–sea CO_2 exchange. Salinity forcing and subsequent estimates of total alkalinity are crude, as are estimates of atmospheric partial pressure. However, despite its limitations a qualitative estimation of air–sea CO_2 exchange is appropriate. Comparison of modelled pCO_2 in the water with data from Goyet et al. (1998) for the same region, indicate that peak modeled values are in the middle of the recorded range during the monsoon period at A1. This gives credence to the models prediction of out-gassing although model estimates are generally significantly higher. Conversely the model suggests draw down at A7 in contrast to outgassing derived by Goyet et al. (1998). Both modelled and measured pCO_2 at A7 show no seasonal signal, although model estimates are slightly lower. Despite inaccuracies, the model confirms the physically driven nature of CO_2 flux into the atmosphere in regions of upwelling, but suggests biologically mediated draw down may be a significant factor in determining the CO_2 flux in regions of downwelling during monsoonally mixed conditions.

There are challenges in validating models of this kind against spatially and temporally specific data

generated on cruise based surveys. As shown by both data and model, the Arabian Sea exhibits considerable heterogeneity in both time and space. This is particularly true comparing the model output with the data generated during the September Arabesque cruise. This is a transitional period when the SW monsoon breaks down and changes of up to an order of magnitude of both biomass and fluxes occur within a short period of time. A second challenge is the provision of forcing functions for the physical model. The day-to-day variability in wind fields is crucial in providing a reasonable degree of mixing in the model and wind patterns are required to determine the spatial trends in the region. It is thus important to use realistic, high-resolution wind data. Although in this case, winds measured during the survey coincide well with the wind forcing used, the actual wind history is unknown. As the behaviour of the system at any given time is complexly linked to the detailed history of wind over the preceding few days, weeks and months, the use of modelled wind forcing must be seen as a possible source of short term error in the model.

5. Conclusions

This modelling exercise illustrates that an ecosystem model developed within the context of temperate shelf sea issues can, without fundamental changes, successfully simulate the mixed layer dynamics of tropical ocean systems and further the dynamics of an extremely heterogeneous system like the Arabian Sea. A key factor is the provision of an accurate physical environment and a model with sufficient complexity to represent microbial, multivorous and classical communities or the continuum of trophic pathways as described by Legendre and Rassoulzadegan (1995). As the ecological model process descriptions and parameters remain constant throughout this study, the results show complex and contrasting communities and exchanges may result from differences in a few basic physical parameters and forcing fields.

Although the differential wind forcing across the region and the proximity of the nutricline to the surface at the onset of mixing events primarily determine the spatial-temporal signal in productivity across the region, the model shows that sub surface chlorophyll maxima are also important and robust areas of production agreeing with Gunderson et al. (1998). The contrasting distributions of nutrients, silicate driven by physical processes, nitrate by a combination of physics and nitrification, ammonium via recycling are shown to be more important in determining large cell community structure. Ecological niches in the latter part of monsoon seasons are created by differential grazing, both herbivorous and carnivorous. Regional trends in microbial community structure are primary driven by the fate of primary production, generally the proportion undergoing short-term lysis. Ecological activity is also suggested to be a significant moderator of CO_2 out gassing in the Arabian Sea interior.

By capturing much of the system's features in a simple 1D approach, the model underlines the usefulness of both fixed and lagrangian long-term water column studies. These provide an important mechanism for the assembly of detailed high frequency process orientated data sets in remote locations, which are crucial to understand the more complex aspects of the system. Indeed simulations of dynamic monsoonally driven events indicate that sampling programs may be severely biased by their precise timing, whilst programs in oligotrophic regions may be more opportunistic in their execution.

Although successful, the model is limited by the lack of horizontal advective processes and resulting turbulent kinetic energy terms. It may also be improved by resolving diurnal physical processes (McCreary et al., 2001). Many developments of the ecosystem model could also be beneficial, for example including coccolithophores, further resolving the phytoplankton or including behavioral and developmental processes for mesozooplankton. The coupling of the ecological model to a fully 3D representation of the Arabian Sea would provide a further test of the ecosystem model and subsequently an extremely powerful tool for quantifying and exploring the Arabian Sea system's dynamics.

Acknowledgements

This research forms part of the Microbially Driven Biogeochemistry programme of the Plymouth Marine Laboratory. It was part funded by Defence Evaluation Research Agency Grant (TQ/10/3/2) as well as the UK Natural Environment Research Council and forms

part of the UK contribution to the SCOR/IGBP JGOFS Arabian Sea Process Study. The authors would also like to acknowledge the constructive and helpful comments made by the anonymous referees.

References

Allen, J.I., Blackford, J.C., Radford, P.J., 1998. An 1-D vertically resolved modelling study of the ecosystem dynamics of the middle and southern Adriatic Sea. Journal of Marine Systems 18, 265–286.

Allen, J.I., Sommerfield, P.J., Siddorn, J., 2001. Primary and bacterial production in the Mediterranean Sea: a modelling study. Journal of Marine Systems (in press).

Angel, M.V., 1984. Marine science of the north-west Indian Ocean and adjacent waters. Deep Sea Research I 31, 573–1035.

Azam, F., Steward, G.F., Smith, D.C., Duklow, H.W., 1994. In: Lal, D. (Ed.), Significance of Bacteria in Carbon Fluxes in the Arabian Sea. Indian Academy of Science, Bangalore, pp. 243–253.

Banse, K., English, D.C., 2000. Geographical differences in seasonality of CZCS derived phytoplankton pigment in the Arabian Sea for 1978–1986. Deep Sea Research II 47, 1623–1677.

Barber, R.T., Marra, J., Bidigare, R.C., Codispoti, L.A., Halpern, D., Johnson, Z., Latasa, M., Goericke, R., Smith, S.L., 2001. Primary productivity and its regulation in the Arabian Sea during 1995. Deep-Sea Research II 48, 1127–1172.

Baretta, J.W., Ebenhoh, W., Ruardij, P., 1995. The European regional seas ecosystem model, a complex marine ecosystem model. Netherlands Journal of Sea Research 33 (3/4), 233–246.

Baretta-Bekker, J., Baretta, J.W., Rasmussen, E., 1995. The microbial food web in the the European regional seas ecosystem model. Netherlands Journal of Sea Research 33, 363–379.

Baretta-Bekker, J.G., Baretta, J.W., Ebenhöh, W., 1997. Microbial dynamics in the marine ecosystem model ERSEM II with decoupled carbon assimilation and nutrient uptake. Journal of Sea Research 38, 195–212.

Barlow, R.G., Mantoura, R.F.C., Cummings, D.G., 1999. Monsoonal influence on the distribution of phytoplankton pigments in the Arabian Sea. Deep-Sea Research II 46, 677–700.

Blumberg, A.F., Mellor, G.L., 1980. A coastal ocean numerical model. In: Sunderman, J., Holtz, K.P. (Eds.), Mathematical Modelling of Estuarine Physics, Proceedings of the International Symposium, Hamburg, Aug. 1978. Springer-Verlag, Berlin, pp. 203–214.

Brock, J., Sathyendranath, S., Platt, T., 1993. Modelling the seasonality of subsurface light and primary production in the Arabian Sea. Marine Ecology Progress Series 101, 209–221.

Broekhuizen, N.R., Heath, M.R., Hay, S.J., Gurney, W.S.C., 1995. Modelling the dynamics of the North Seas mesozooplankton. Netherlands Journal of Sea Research 33 (3/4), 381–815.

Buesseler, K., Ball, L., Andrews, J., Benitez-Nelson, C., Belastock, R., Chai, F., Chao, Y., 1998. Upper ocean export of particulate organic carbon in the Arabian Sea derived from thorium-234. Deep-Sea Research II 46, 2461–2488.

Burkill, P.H., 1999a. ARABESQUE: UK JGOFS process studies in the Arabian Sea. Deep Sea Research II 46, 529–863.

Burkill, P.H., 1999b. ARABESQUE: an overview. Deep-Sea Research II 46, 529–548.

Burkill, P.H., Mantoura, R.F.C., Owens, N.J.P., 1993a. Biogeochemical cycling in the northwestern Indian Ocean: a brief overview. Deep-Sea Research II 40, 643–650.

Burkill, P.H., Leakey, R.J.G., Owens, N.J.P., Mantoura, R.F.C., 1993b. Synechococcus and its importance to the microbial foodweb of the northwestern Indian Ocean. Deep-Sea Research II 40, 773–782.

Carlson, C.A., Ducklow, H.W., Michaels, A.F., 1994. Annual flux of dissolved organic carbon from the euphotic zone in the northwestern Sargasso Sea. Nature 371, 405–408.

Copin-Montegut, G., Avril, B., 1993. Vertical distribution and temporal variation of dissolved organic carbon in the north–west Mediterranean Sea. Deep-Sea Research I 40, 1963–1972.

Dickey, T., Marra, J., Sigurdson, D.E., Weller, R.A., Kinkade, C.S., Zedler, S.E., Wiggert, J.D., Langdon, C., 1998. Seasonal variability of bio-optical and physical properties in the Arabian Sea: October 1994–October 1995. Deep-Sea Research II 45, 2001–2026.

Dickson, M.-L., Orchardo, J., Barber, R.T., Marra, J., McCarthy, J.J., Sambrotto, R.N., 2001. Production and respiration rates in the Arabian Sea during the 1995 Northeast and Southwest Monsoons. Deep-Sea Research II 48, 1199–1230.

Dobson, F.W., Smith, S.P., 1988. Bulk models of solar radiation at sea. Quarterly Journal of the Royal Meteorological Society 114, 165–182.

Ducklow, H.W., 1993. Bacterioplankton distributions and production in the northwestern Indian Ocean and Gulf of Oman, September 1986. Deep-Sea Research II 40, 753–772.

Ducklow, H.W., Smith, D.C., Campbell, L., Landry, M.R., Quinby, H.L., Steward, G.F., Azam, F., 2001. Heterotrophic bacterioplankton in the Arabian Sea: Basinwide response to yearround high primary productivity. Deep-Sea Research II 48, 1303–1324.

Ebenhöh, W., Baretta, J.W., Baretta-Bekker, J.G., 1997. The primary production model in a marine ecosystem model ERSEM II. Journal of Sea Research 38, 169–172.

Edwards, E.S., Burkill, P.H., Stelfox, C.E., 1999. Zooplankton herbivory in the Arabian Sea during and after the SW monsoon, 1994. Deep-Sea Research II 46, 843–863.

Findlater, J., 1974. The low-level cross equatorial air current of the western Indian Ocean during the northern summer. Weather 29, 411–416.

Fischer, A.S., 2000. Ph.D. Dissertation, Massachusetts Institute of Technology-Woods Hole Oceanographic Institute, 222.

Gage, J.D., Levin, L.A., Wolff, G.A., 2000. Benthic processes in the Deep Arabian Sea. Deep Sea Research II 47, 1–7.

Gardner, W.D., Gundersen, J.S., Richardson, M.J., Walsh, I.D., 1999. The role of seasonal and diel changes in mixed-layer depth on carbon and chlorophyll distributions in the Arabian Sea. Deep-Sea Research II 46, 1833–1858.

Garrison, D.L., Gowing, M.M., Hughes, M.P., Campbell, L., Caron,

D.A., Dennett, M.R., Shalapyonok, A., Olson, R.J., Landry, M.R., Brown, S.L., Liu, H.-B., Azam, F., Steward, G.F., Ducklow, H.W., Smith, D.C., 2000. Microbial food web structure in the Arabian Sea: a US JGOFS study. Deep-Sea Research II 47, 1387–1422.

Goyet, C., Millero, F.J., O'Sullivan, D.W., Eischeid, G., McCue, S.J., Bellerby, R.G.J., 1998. Temporal variations of pCO_2 in surface seawater of the Arabian Sea in 1995. Deep-Sea Research I 45 (4–5), 609–624.

Gunderson, J.S., Gardner, W.D., Richardson, M.J., Walsh, I.D., 1998. Effects of monsoons on the seasonal and spatial distributions of POC and chlorophyll in the Arabian Sea. Deep-Sea Research II 45, 2103–2132.

Halpern, D., Freilich, M.H., Weller, R.A., 1998. Arabian Sea surface winds and ocean transports determined from ERS-1 scatterometer. Journal of Geophysical Research-Oceans 103, 7799–7806.

Hansell, D.A., Peltzer, E.T., 1998. Spatial and temporal variations of total organic carbon in the Arabian Sea. Deep-Sea Research II 45, 2171–2194.

Hansson, I., 1973. A new set of pH scales and standard buffers for sea water. Deep-Sea Research I 20, 479–491.

Honjo, S., Dymond, J., Prell, W., Ittekkot, V., 1999. Monsoon controlled export fluxes to the interior of the Arabian Sea. Deep-Sea Research II 46, 1859–1902.

Jochem, F.J., Pollehne, F., Zeitzschel, B., 1993. Productivity regime and phytoplankton size structure in the Arabian Sea. Deep-Sea Research II 40, 711–736.

Keen, T.R., Kindle, J.C., Young, D.K., 1997. The interaction of southwest monsoon upwelling, advection and primary production in the northwest Arabian Sea. Journal of Marine Systems 13, 61–82.

Kindle, J.C., 2002. The surface circulation of the northern Arabian Sea. In: Watts, L., Burkill, P.H., Smith, S.L. (Eds.). Report of the Indian Ocean Synthesis Group on the Arabian Sea Process Study. JGOFS Report 35, 1–114.

Kinkade, C.S., Marra, J., Dicky, T.D., Weller, R., 2001. An annual cycle of phytoplankton biomass in the Arabian Sea, 1994–1995, as determined by moored optical sensors.

Körtzinger, A., Duinker, J.C., Mintrop, L., 1997. Strong CO_2 emissions from the Arabian Sea during the south–west monsoon. Geophysical Research Letters 24, 1763–1766.

Landry, M.R., Brown, S.L., Campbell, L., Constantinou, J., Liu, H.B., 1998. Spatial patterns in phytoplankton growth and microzooplankton grazing in the Arabian Sea during monsoon forcing. Deep-Sea Research II 45, 2353–2368.

Latasa, M., Bidigare, R.R., 1998. A comparison of phytoplankton populations of the Arabian Sea during the spring intermonsoon and Southwest monsoon of 1995 as described by HPLC-analyzed pigments. Deep-Sea Research II 45, 2133–2170.

Lee, C.M., Jones, B.H., Brink, K.H., Fischer, A.S., 2000. The upper-ocean response to monsoonal forcing in the Arabian Sea: seasonal and spatial variability. Deep-Sea Research II 47, 1177–1226.

Legendre, L., Rassoulzadegan, F., 1995. Plankton and nutrient dynamics in marine waters. Ophelia 41, 153–172.

Lenhart, H.J., Radach, G., Ruardij, P., 1997. The effects of river input on the ecosystem dynamics in the continental coast zone of the North Sea using ERSEM. Journal of Sea Research 38, 249–274.

Liss, P.S., Merlivat, L., 1986. Air–sea gas exchange rates: introduction and synthesis. In: Buat-Menard, P. (Ed.), The role of Air–Sea Exchange in Geochemical Cycling. D. Reidel, Dordrecht, pp. 113–127.

Madhupratap, M., Gopalakrishnan, T.C., 1996. Lack of seasonal and geographic variation in mesozooplankton biomass in the Arabian Sea and its structure in the mixed layer. Current Science 71, 863–868.

Marra, J., Dickey, T.D., Ho, C., Kinkade, C.S., Sigurdson, D.E., Weller, R.A., Barber, R.T., 1998. Variability in primary production as observed from moored sensors in the central Arabian Sea in 1995. Deep-Sea Research I 45, 2253–2268.

McCreary, J.P., Kohler, K.E., Hood, R.R., Olson, D.B., 1996. A four component ecosystem model of biological activity in the Arabian Sea. Progress in Oceanography 37, 193–240.

McCreary, J.P., Kohler, K.E., Hood, R., Smith, S., Kindle, J., Fischer, A., Weller, R.A., 2001. Influences of diurnal and intraseasonal forcing on mixed-layer and biological variability in the central Arabian Sea. Journal of Geophysical Research 106, 7139–7155.

Mellor, G.L., Yamada, T., 1982. Development of a turbulence closure model for geophysical fluid problems. Reviews of Geophysics and Space Physics 20 (4), 851–875.

Millero, F.J., Lee, K., Roche, M., 1998. Distribution of alkalinity in the surface waters of the major oceans. Marine Chemistry 60, 111–130.

Mintrop, L., Körtzinger, A., Duinker, J.C., 1999. The carbon dioxide system in the northwestern Indian Ocean during the south–west monsoon. Marine Chemistry 64, 315–336.

Owens, N.J.P., Burkill, P.H., Mantoura, R.F.C., Woodward, E.M.S., Bellan, I.E., Aiken, J., Howland, R.J.M., Llewellyn, C.A., 1993. Size-fractionated primary production and nitrogen assimilation in the northwestern Indian Ocean. Deep-Sea Research II 40, 697–710.

Patsch, J., Radach, G., 1997. Long term simulation of the eutrophication of the North Sea: temporal development of nutrients, chlorophyll and primary production in comparison to observations. Journal of Sea Research 38, 275–310.

Pfannkuche, O., Lochte, K., 2000. The Biogeochemistry of the Deep Arabian Sea. Deep Sea Research II 47, 2615–2628.

Pollehne, F., Klein, B., Zeitzschel, B., 1993. Low light adaptation and export production in the deep chlorophyll maximum layer in the northern Indian Ocean. Deep-Sea Research II 40, 737–752.

Pomroy, A., Joint, I., 1999. Bacterioplankton activity in the surface waters of the Arabian Sea during and after the 1994 SW monsoon. Deep-Sea Research II 46, 767–794.

Reckermann, M., 1996. Ultraphytoplankton and protozoan communities and their interactions in different marine pelagic ecosystems (Arabian Sea and Baltic Sea). Meereswissenschaftliche Berichte Warnemunde 14, 139 pp.

Reckermann, M., Veldhuis, J.W., 1997. Trophic interactions between picophytoplankton and micro- and nanozooplankton in the western Arabian Sea during the NE monsoon 1993. Aquatic Microbial Ecology 12, 263–273.

Rixen, T., Haake, B., Ittekkot, V., 2000. Sedimentation in the western Arabian Sea the role of coastal and open-ocean upwelling. Deep-Sea Research II 47, 2155–2178.

Robinson, C., Williams, P.J.LeB., 1999. Plankton net community production and dark respiration in the Arabian Sea during September 1994. Deep-Sea Research II 46, 745–766.

Rochford, P.A., Kindle, J.C., Gallacher, P.A., 2000. Sensitivity of the Arabian Sea mixed layer to 1994–1995 operational wind products. Journal of Geophysical Research 105, 14141–14162.

Roman, M., Smith, S., Wishner, K., Zhang, X., Gowing, M., 2000. Mesozooplankton production and grazing in the Arabian Sea. Deep-Sea Research II 47, 1423–1450.

Ruardij, P., Baretta, J.W., Baretta-Bekker, J.G., 1995. SESAME: a software environment for simulaton and analysis of marine ecosystems. Netherlands Journal of Sea Research 33 (3/4), 261–270.

Ryabchenko, V.A., Gorchakov, V.A., Fasham, M.J.R., 1998. Seasonal dynamics and biological productivity in the Arabian Sea euphotic zone as simulated by a three-dimensional model. Global Biogeochemical Cycles 12, 501–530.

Savidge, G., Gilpin, L., 1999. Seasonal influences on size fractionated chlorophyll a concentrations and primary production in the north–west Indian Ocean. Deep-Sea Research II 46, 701–724.

Schott, F.J., McCreary, J.P., 2001. The monsoon circulation of the Indian Ocean. Progress in Oceanography 51, 1–123.

Shi, W., Morrison, J.M., Böhm, E., Manghnani, V., 2000. The Oman upwelling zone during 1993, 1994 and 1995. Deep-Sea Research II 47, 1227–1248.

Smith, S.L., 1998. The 1994–1996 Arabian Sea expedition: oceanic response to monsoonal forcing, part 1. Deep-Sea Research II 45, 1905–2501.

Smith, S.L., 1999. The 1994–1996 Arabian Sea expedition: oceanic response to monsoonal forcing, part 2. Deep-Sea Research II 46, 1532–1964.

Smith, S.L., 2000. The 1994–1996 Arabian Sea expedition: oceanic response to monsoonal forcing, part 3. Deep-Sea Research II 47, 1177–1677.

Smith, S.L., 2001. The 1994–1996 Arabian Sea expedition: oceanic response to monsoonal forcing, part 4. Deep-Sea Research II 48, 1069–1402.

Smith, S.L., Codispoti, L.A., Morrison, J.M., Barber, R.T., 1998a. The 1994–1996 Arabian Sea Expedition: an integrated, interdisciplinary investigation of the response of the northwestern Indian Ocean to monsoonal forcing. Deep-Sea Research II 45, 1905–1915.

Smith, S., Roman, M., Prusova, I., Wishner, K., Gowing, M., Codispoti, L.A., Barber, R., Marra, J., Flagg, C., 1998b. Seasonal response of zooplankton to monsoonal reversals in the Arabian Sea. Deep-Sea Research II 40, 2369–2404.

Sorokin, Y.I., Kopylov, A.I., Mamaeva, N.V., 1985. Abundance and dynamics of microzooplanktonin the central tropical Indian Ocean. Marine Ecology Progress Series 24, 27–41.

Stelfox, C.E., Burkill, P.H., Edwards, E.S., Harris, R.P., Sleigh, M.A., 1999. The structure of zooplankton communities, in the 2 to 2000 μm size range, in the Arabian Sea during and after the SW monsoon, 1994. Deep-Sea Research II 46, 815–842.

Swallow, J., 1991. Circulation in the northwestern Indian Ocean. In: Smith, et al. (Eds.). US JGOFS Arabian Sea Process Study Planning Report 13, pp. 37–39.

Tarran, G.A., Burkill, P.H., Edwards, E.S., Woodward, E.M.S., 1999. Phytoplankton community structure in the Arabian Sea during and after the SW monsoon, 1994. Deep-Sea Research II 46, 655–676.

Taylor, A.H., Watson, A.J., Ainsworth, A., Robertson, J.E., Turner, D.R., 1991. A modelling investigation of the role of phytoplankton in the balance of carbon at the surface of the North Atlantic. Global Biogeochemical Cycles 5 (2), 151–171.

Thingstad, T.F., Hagstrom, A., Rassoulzadegan, F., 1997. Accumulation of degradable DOC in surface waters: is it caused by a malfunctioning of the microbial loop? Limnology and Oceanography 42, 398–404.

Van Weering, T.C.E., Helder, W., Schalk, P., 1997. Netherlands Indian Ocean program (1992–1993) first results. Deep Sea Research II 44, 1177–1193.

Vichi, M., Pinardi, N., Zavatarelli, M., Matteucci, G., Marcaccio, M., Bergamini, M.C., Frascari, F., 1998a. One dimensional ecosystem model results in the Po prodelta area (northern Adriatic Sea). Environmental Modelling and Software 13, 471–481.

Vichi, M., Zavatarelli, M., Pinardi, N., 1998b. Seasonal modulation of microbially mediated carbon fluxes in the northern Adriatic Sea—a model study. Fisheries. Oceanology. Journal of Marine Systems 7, 182–190.

Watts, L.J., Owens, N.J.P., 1999. Nitrogen assimilation and the f-ratio in the north-western Indian Ocean during an intermonsoon period. Deep-Sea Research II 46, 725–744.

Watts, L., Burkill, P.H., Smith, S.L., 2002. Report of the Indian Ocean Synthesis Group on the Arabian Sea Process Study. JGOFS Report 35, 1–114.

Weiss, F., 1970. The solubility of nitrogen, oxygen and argon in water and seawater. Deep Sea Research 17, 721–735.

Weiss, R.F., 1974. Carbon dioxide in water and sea water: the solubility of a non-ideal gas. Marine Chemistry 2, 203–215.

Weisse, T., 1999. Bactivory in the north-western Indian Ocean during the intermonsoon-north–east monsoon period. Deep-Sea Research II 46, 795–814.

Weller, R.A., Baumgartner, M.F., Josey, S.A., Fischer, A.S., Kindle, J.C., 1998. Atmospheric forcing in the Arabian Sea during 1994–1995: observations and comparisons with climatology and models. Deep-Sea Research II 45, 1961–2000.

Wiebinga, C.J., Veldhuis, M.J.W., De Baar, H.J.W., 1997. Abundance and productivity of bacterioplankton in relation to seasonal upwelling in the northwest Indian Ocean. Deep-Sea Research I 44, 451–476.

Wiggert, J.D., Jones, B.H., Dickey, T.D., Brink, K.H., Weller, R.A., Marra, J., Codispoti, L.A., 2000. The Northeast Monsoon's impact on mixing, phytoplankton biomass and nutrient cycling in the Arabian Sea. Deep-Sea Research II 47, 1353–1386.

Williams, P.J.LeB., 1995. Evidence for seasonal accumulation of carbon-rich dissolved organic material, its scale in comparison with changes in particulate material and the consequential effect on net C/N assimilation ratios. Marine Chemistry 51, 17–29.

Woodward, E.M.S., Rees, A.P., Stephens, J.A., 1999. The influence of the SW monsoon upon the nutrient biogeochemistry of the Arabian Sea. Deep-Sea Research II 46, 571–592.

Yoder, J.A., McClain, C.R., Feldman, G.C., Esaias, W.E., 1993. Annual cycles of phytoplankton chlorophyll concentrations in the global ocean: a satellite view. Global Biogeochemical Cycles 7, 181–193.

Young, D.K., Kindle, J.C., 1994. Physical processes affecting availability of dissolved silicate for diatom production in the Arabian Sea. Journal of Geophysical Research 99, 22619–22632.

Zavaterelli, M., Baretta, J.W., Baretta-Bekker, J.G., Pinardi, N., 2000. The dynamics of the Adriatic Sea ecosystem. An idealized model study. Deep-Sea Research I 47, 937–970.